BIRZEIT UNIVERSITY

Faculty of Science كليـة العلـوم

Department of Physics دائـرة الفيـزيـاء

Physical Pendulum Viscometer: A Method for Quantifying Liquids' Viscosity

البندول الفيزيائي كأداة لقياس و تحديد لزوجة السوائل

By:

Rand Fuad Aqra

Supervised by:

Dr Khalid Eid

Birzeit, Palestine

June, 2022

Physical Pendulum Viscometer: A Method for Quantifying Liquids' Viscosity

البندول الفيزيائي كأداة لقياس و تحديد لزوجة السوائل

By:

Rand Fuad Aqra

Thesis committee:

Dr Khalid Eid (Principal advisor).

Prof Ahmed Abu Hanieh (Member).

Dr Hazem AbuSara (Member).

This thesis was submitted in partial fulfillment of the requirements for the Master's Degree in Physics from the Factually of Graduate Studies at Birzeit, Palestine.

June 2022

Physical Pendulum Viscometer: A Method for Quantifying Liquids' Viscosity

By: Rand Fuad Aqra

Accepted by the Factually of Graduate Studies, Birzeit University,

in partial fulfillment of the requirements for the Master's Degree in Physics.

Thesis committee:

Dr Khalid Eid (Principal advisor).

……

Prof Ahmed Abu Hanieh (Member).

……

Dr Hazem AbuSara (Member).

……

June 2022

Dedication

في مرحلةٍ ما من هذه الحياة، قد يسأل المرء نفسه: من أنا؟

أما أنا، وفي هذه اللحظة من حياتي: إذ اسأل نفسي ذات السؤال.

أجد ذات الإجابة البديهية.

أنا دعاؤكما،

نصائحكما،

و دعمكما المستمر في شتى الظروف.

أنا صورتي عندما أنظر في عينيكما أو عيني أحدكما.

أنا رند فؤاد نادية

أهدي جهدي وتعبي هذا إلى من لا أجد تعريفاً لنفسي دونهما؛ إلى نادية إبراهيم اقرع، أمي، وفؤاد عيسى اقرع، أبي. و كما أهديه إلى أجمل الهدايا التي منحوني اياها: أخوتي و أخواتي وعائلاتهم.

و آخر دعواي أن الحمدلله رب العالمين

Acknowledgment

I would like to express my gratitude to my teacher, advisor, and supervisor Dr Khalid Eid for all the help, guidance, and support during this thesis work and during my years as a physics graduate student. Also, I would like to thank the committee members Prof Ahmed Abu Hanieh and Dr Hazem AbuSara.

Special thanks to Eng. Jamal Sobaih, and Eng. Ahmad Jara from the workshops of the Mechanical and Mechatronics Engineering department for all their help in the fabrication of the new instrument. To Eng. Alaaleddin Qarqash from the fluid mechanics' laboratories of the Mechanical and Mechatronics Engineering department for all the valuable discussions and notes. To Eng. Shadi K'Aibni from the Testing Laboratories Center at Birzeit University for providing us with the different liquids used in this thesis. To Mr. Ibrahim Shalash and Mr. Azmi Dudin from the Chemistry department for providing us with the capillary viscometer used in this thesis. And to Physics department laboratories technicians Mr. Sami Naser and Eng. Al-Mothana Ahmed for their efforts during the development of this experimental project.

Finally, I would like to thank my colleagues and friends, especially Khattab AbualRob for his help and valuable and powerful discussions during this project and other projects, and Ahlam Abd Eljalil for her help in this project.

Abstract

We developed and fabricated a new viscometer. This new viscometer has been designed and developed for measuring the viscosity of any liquid even the high viscous liquids, and it can be used to measure the magneto-viscosity of the magnetorheological fluids and ferrofluids and to measure the viscosity of the non-Newtonian fluids. In this project, the measurements were based on the study of the damping mechanism and observation of the damped motion on the physical pendulum, and derivation of the viscosity by three different analyzing methods: the energy-loss curves, the damping constant, and the period of oscillations. The results appear that we have developed a precise and accurate instrument to measure the viscosity with an error percentage of ± 8 % of the viscosity in light liquids and ± 0.5 % of the viscosity in high viscous liquids.

الملخص

لقد قمنا بتصميم و تطوير مقياس لزوجة جديد. تم تصميم و تطوير و تصنيع مقياس اللزوجة هذا لقياس لزوجة أي سائل بما يشمل السوائل ذات اللزوجة المرتفعة، إذ أنه بالإمكان استخدام هذا المقياس لقياس اللزوجة المغناطيسية للسوائل المغناطيسية و السوائل الممغنطة، وقياس لزوجة السوائل غير النيتونية. استندت القياسات في هذه الدارسة على دراسة آلية التخميد و مراقبة الحركة المثبطة للبندول الفيزيائي الذي قمنا بتصميمه، حيث أنه تم اشتقاق اللزوجة من خلال ثلاثة طرق تحليل مختلفة: باستخدام منحنيات فقدان الطاقة، باستخدام ثابت التخميد، و من خلال التغير في فترة الذبذات. تظهر النتائج أننا قمنا بتطوير أداة دقيقة و صحيحة لقياس لزوجة السوائل بنسبة خطأ تبلغ % 8 ± من قيمة اللزوجة في السوائل الخفيفة، و % 0.5 ± من قيمة اللزوجة في السوائل عالية اللزوجة.

Table Of Contents

Table Of Figures

Table Of Tables

1 Introduction

Fluids are substances that can flow and are made of randomly arranged molecules. Besides the liquids, gases, and plasma, some types of fine powders can also behave like fluids (Royer, et al. 2007, Ziaee and Crane 2019). Fluid mechanics is the branch of physics, specifically continuum mechanics, that studies the mechanisms of fluid flow and the forces upon them. Flow depends on two main properties of the fluid: density and viscosity.

Hand-waving is an easy movement we can do in the air, but what about if we try to slide our hand in the water? The movement becomes harder and the same happens in other liquids such as oils, mercury, or ethylene glycol. This is determined by the fluid's deformation/strain rate at specified shear stress. The applied shear stress is usually linearly proportional to the fluid's strain rate (velocity gradient) (Serway and Jewett, Jr. 2014, Viswanath 2007, White 2009). The proportionality constant of this relation is called the dynamic viscosity which can be defined as the fluid's internal resistance to flow (White 2009).

Let's consider a simple two-layer system shown in figure 1.2, the upper layer drifts slowly to the side and subjects the fluid to an applied force, this force per unit area is the shear stress which is parallel to the layer surface. The lower layer was fixed. The velocity gradient in this simple system is the velocity divided by the distance between the two layers (y). In general, the dynamic viscosity is mathematically expressed as in equation 1-1.

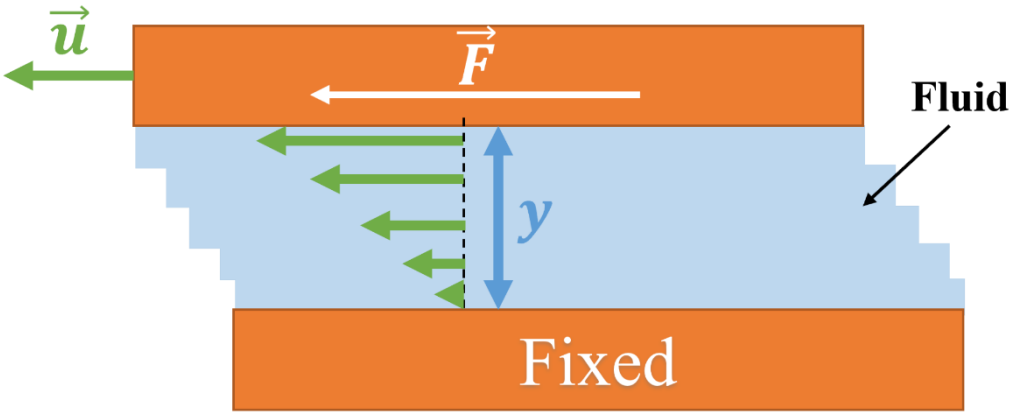

Figure 1.1.1: Shear on a two-layer fluid film.

$$\eta = \frac{\tau}{\frac{du}{dy}} \qquad 1\text{-}1$$

Where η is the dynamic viscosity, τ is the shear stress, and du/dy is the strain rate (velocity gradient) (Viswanath 2007, White 2009). The dynamic viscosity has the units of stress multiplied by time or $(Pa.s)$. A slightly different definition of viscosity comes from the fact that the force equals the rate of change of momentum ($F = ma = \Delta p/\Delta t$) (Serway and Jewett, Jr. 2014). So, the rate of momentum transport per unit area (the momentum flux) is proportional to the fluid's strain rate (velocity gradient). In this case, the proportionality constant is called the kinematic viscosity (υ) and is defined as the fluid's tendency to transport momentum (Viswanath 2007, White 2009).

$$\upsilon = \frac{\tau}{\frac{d(\rho u)}{dy}} = \frac{\eta}{\rho} \qquad 1\text{-}2$$

Where ρ is the fluid's density.

However, not all fluids obey equations (1-1) or (1-2). After the year 1687 when Sir Isaac Newton postulated the viscosity concept and law experimentally, the fluids that obeyed this law (1-1) came to be called Newtonian fluids (Viswanath 2007, White 2009, Irgens 2014). These include most of the common fluids like gases and simple liquids including water, oils, and liquid metals. On the other hand, fluids that do not obey this law are called non-Newtonian fluids. These fluids include polymer solutions, slurries, and paints (Irgens 2014). In this case, the shear stress is not linearly proportional to the strain rate. The proportionality between the shear stress and the strain rate in the case of the non-Newtonian fluids differs with the fluid type, which can be classified into two main types:

1- The time-independent fluids, whose viscosity changes with changing the applied shear stress. According to the viscosity behavior, this type contains three subgroups:
a) The shear-thinning fluids (PsuedoPlastic), where the viscosity decreases with increasing the stress.

b) The shear-thickening fluids (dilatant), where the viscosity increases with increasing the shear stress

c) The Bingham fluids (Rheological fluids), where the shear rate equals zero if the applied stress is smaller than or equal to a certain value (τ_0), and is directly proportional to the strain rate at larger shear stress (Viswanath 2007, Irgens 2014).

2- The second type was the time-dependent fluids, in which the viscosity under constant strain rate changes with time (Viswanath 2007, Irgens 2014).

The viscosity of Newtonian fluids is a thermodynamic property that varies with changing temperature and pressure. It increases weakly with increasing the pressure, while the temperature has a larger effect on the viscosity depending on the fluid's state. In gases at low densities, the viscosity increases as $\sqrt{T}$ with increasing the temperature according to the ideal gas law (Viswanath 2007). Whereas in liquids, viscosity decreases with increasing the temperature, since the intermolecular cohesive forces decrease with it.

1.1 Viscometers and Viscosity measurements

Determining the viscosity of different fluids is important both in research and industrial applications. In industry, it is important in processing, and product quality testing, especially in the plastic industry (Viswanath 2007). It is also important in the food (Sharma, et al. 2015, Bista, et al. 2021), medicine (Muriel and Katz 2021), and motor oils industries (Hameed 2021). Determining a fluid's viscosity is also important in many research fields like measuring the magneto-viscosity of magnetic fluids that can be utilized in applications like door-stops and car suspension systems.

Many instruments -known as viscometers- were developed to study and measure the fluids' flow and viscosity. Some viscometers measure the dynamic viscosity by studying the fluid's resistance to flow under controlled external forces. Others observe the fluid's resistance to flow under gravity in order to measure the kinematic viscosity. Among the many types of viscometers that were developed and used over the years are the capillary, the rotational, the falling ball, and the vibrational

viscometers (Viswanath 2007). Many conditions can play an important role in choosing the viscometer type such as the range of measurements, the fluid's type either Newtonian or non-Newtonian, temperature control, and the type of flow, among other qualifications.

1.2 Drag Force and Viscosity Proportionality

Even though the viscosity depends on the drag force, we cannot simply say that the drag force is proportional to the viscosity or vice versa. They have a complex proportionality which is separated into many regimes, depending on velocity, object's shape, and fluid. A parameter known as the Reynolds number is defined to determine these regimes (Reynolds 1883, Sommerfeld 1908).

$$Re = \frac{d\rho v}{\eta} \qquad 1\text{-}3$$

Where "Re" is the Reynolds number, d is the object's diameter, ρ is the fluid's density, v is the object's velocity, and η is the fluid's dynamic viscosity.

We generally can define three main flow regimes according to the Reynolds number and the flow rate (velocity).

1- At low velocities such that "Re" becomes smaller than one, the flow will be highly laminar and the viscous drag force is entirely coming from the fluid's viscosity. This drag force directly depends on the viscosity and the object's velocity, as quantified by the Stokes low (Stokes 1851).

$$F_d^{viscous} = a\eta v \qquad 1\text{-}4$$

Where a 'a measure of the object's size' and is equal to 6πr for a sphere.

2- At large velocities, unusual fluids, or unusual object shapes, the Reynolds' number "Re" can be larger than 10000. This drag force comes from the inertial drag and is proportional to the square of the object's velocity multiplied by the fluid's density. In this case, the flow will be turbulent, and the viscous drag force will be negligible.

$$F_d^{inertial} = \frac{C_D S}{2} \rho v^2 \qquad 1\text{-}5$$

Where S is the object's cross-sectional area and C_D is the drag coefficient.

3- When "Re" is in the range between these two values (i.e. between 1 and 10,000), the two forces will have to be considered, since both of them contribute to the total drag force, and this is called the transition regime. This regime is actually divided into multiple regimes according to the Reynolds number order of magnitude: the laminar regime when "Re" lies between 1 and 100, the weak laminar regime $(100 < Re < 1000)$, and transition to a turbulent regime $(10^3 < Re < 10^4)$ (White 2009). In this project, we are interested in the highly laminar and the laminar regimes.

1.3 Pendulum Viscometers

As mentioned before, Newton experimentally established that the damping of the oscillations of a pendulum immersed in a fluid is related to the fluid's density and viscosity. Almost two centuries later, Stokes studied this proportionality and theoretically derived equation (*1-4*) known as Stokes law. This equation describes the effect of the viscous drag force on the pendulum's oscillations (Stokes 1851). His paper included the study of a moving sphere in a fluid at low velocities and linked the viscous drag force with the viscosity linearly. After that, Reynolds in 1883

(Reynolds 1883) and then Sommerfeld in 1908 (Sommerfeld 1908) studied the limitations on the validity of the Stokes law and defined the Reynolds number as a means to determine when the Stokes law is valid and when it is not. The following years through the 20th and 21st centuries witnessed many experimental and analytical studies on the proportionality of the damping of under-liquid pendulum with the viscosity. These studies included the study of many types of under-liquid pendulums as studying the oscillations of torsion pendulums to find the viscosity (Hong and Lu 1995), studying the effects of viscous fluids on simple pendulum oscillations (Zonetti, et al. 1999, Hou, et al. 2015), and using simple or physical pendulums as viscometers (Janik, et al. 2006, Rudyak, et al. 2008, Leme and Oliveira 2017). Most of these studies focused on small oscillation angles, (i.e. low velocities) where the viscous drag force and Stokes law are valid. Furthermore, the under-liquid pendulum oscillations were also studied for various other objectives such as studying the dynamics of an inverted pendulum underwater for energy harvesting (Hasnain, et al. 2020), using it in studying the fluid-structure interactions (Martins, Silveira-Neto and Steffen Jr 2007, Bos and Wellens 2021), and using the pendulum motion to estimate the hydrodynamics of underwater vehicles (Yh and Lau 2008).

In this thesis, we developed a new pendulum-based viscometer that was carefully designed to measure extremely low angles, scale down the torque caused by the liquid's drag force to control the damping rate, and is easily analyzed by automating the data collection and analysis. The extremely lightweight of the thin hollow aluminum cylinder gives the device extraordinary sensitivity.

2 Theoretical Background

The use of a physical pendulum to measure liquids' viscosity through damping requires a detailed understanding of the possible damping mechanisms in the pendulum. Let's consider a simple physical pendulum as shown in Figure 2.1 which oscillates with a period of T_o and is affected by a damping torque that comes from the drag or frictional force (F_r) acting on the pendulum arm. Taking into account the small-angle approximation, the equation of motion for this physical pendulum is:

$$\sum \tau = I\ddot{\theta} \qquad 2\text{-}1$$

So, assuming the drag force acts at the tip of the pendulum:

$$I\ddot{\theta} + F_r L + mgL_{CM}\theta = 0 \qquad 2\text{-}2$$

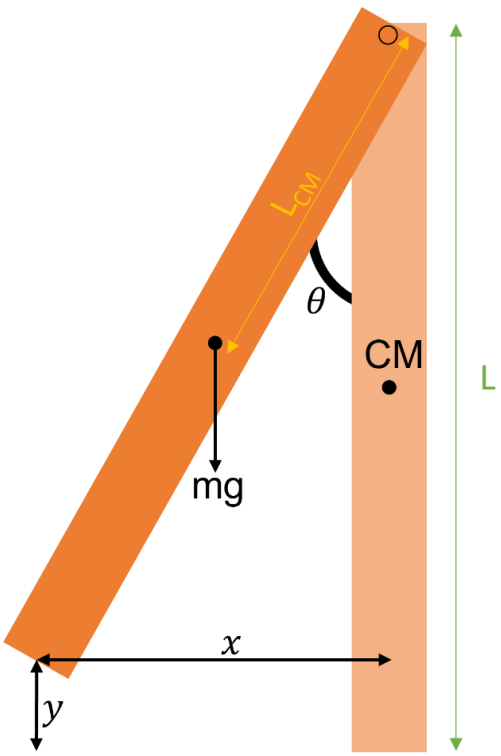

Figure 2.1: Sketch of a physical pendulum.

Where θ is the oscillating angle, τ is the torque, I is the moment of inertia and equals $\int_V \rho\, L^2 dV = 2\pi r^2 \int_0^{L_{cm}} L^2 dL = \frac{1}{3} m L_{CM}^2$ which is valid for a rigid physical pendulum and a long thin hollow cylinder, m is the mass of the pendulum, and L_{CM} is the pendulum's center of mass position.

The pendulum's damping mechanism differs with different drag force types. Usually, it is described with an analytically solvable model of drag force linearly proportional to the angular velocity. This force gives an exponential decay in the oscillation amplitude. Yet, there are other forms of drag that require a more practical and comprehensive mathematical treatment. Particularly, we will consider three different types of drag force (all of which are always in the direction opposite to motion):

1- The velocity-independent frictional force $F_r = f_0 \hat{v}$. This constant damping force appears on the fulcrum point and causes a linear decay in the amplitude of the oscillations.

2- The linear drag force (i.e. $F_r = f_1 v \hat{v}$), which is the best known and treated type of drag force. This type corresponds to small Reynolds numbers and is known as the viscous drag force or Stokes law (equation 1-4).

3- The quadratic drag force, which is proportional to the square of the velocity (i.e. $F_r = f_2 v^2 \hat{v}$). This type corresponds to air drag at high velocities and large Reynolds numbers. This force is known as the inertial drag force and is defined by equation 1-5.

A real physical pendulum is ordinarily affected by a combination of these three forces, thus giving rise to the following equation of motion:

$$\ddot{\theta} + \gamma_2|\dot{\theta}|\dot{\theta} + 2\gamma_1\dot{\theta} + f_0 + \omega_0^2\theta = 0 \qquad 2\text{-}3$$

Here γ_2 is the quadratic force damping constant, γ_1 is the linear force damping constant, and ω_0^2 is the pendulum's normal angular frequency.

2.1 Energy-Based Analysis

Equation 2-3 is not solvable using the analytical differential-equations-based methods. So, a realistic treatment has been developed in the 1970s (Miller 1974, Crawford 1975, Squire 1986) to solve the pendulum's equation of motion under the effect of various frictional/drag force types, which can be used to determine the type of the frictional/drag force acting on the pendulum. This method is energy-based and relies on finding the energy loss per cycle due to the damping or drag forces. It is well-known that if a pendulum starts the oscillations from an angular position θ_n, it will not exceed that same position after completing a period of oscillations, due to energy conservation, and it will start the new period from a new angular position θ_{n+1}. The difference in these positions ($\Delta\theta$) is related to the amount of loss in mechanical energy (ΔE) over a complete period of oscillations. This loss is equal to the work done ($d\vec{w}$) by the frictional forces ($\vec{F}$) over a distance $d\vec{\theta}$ ($dw = \vec{F}.d\vec{\theta}$), and according to the work-energy theorem, ΔE equals

$$\Delta E = \int_0^T \vec{F}.\vec{v}\, dt \qquad 2\text{-}4$$

Where $\vec{v}$ is the velocity and equals $L\dot{\vec{\theta}}$, and T is the period of oscillations. Assuming that $\theta = A\ cos\,(\omega t + \phi)$, $\dot{\theta}\ =\ -A\omega\ sin\,(\omega t)$, where A is the amplitude of oscillations, ω is the angular frequency and equals $\frac{2\pi}{T}$, and ϕ is a phase shift.

We also know that the average energy of a pendulum during a complete cycle/period of oscillations equals

$$E = < E > = \int_0^T E_T(t)\, dt \qquad 2\text{-}5$$

Where $E_T(t)$ is the total mechanical energy and equals the summation of the kinetic energy ($\frac{1}{2}mv^2$) and the potential energy (mgh). So,

$$E = \frac{1}{2}m\omega^2 A^2 \qquad 2\text{-}6$$

And thus, the amount of energy loss (ΔE) is:

$$\Delta E = m\omega^2 A\ \Delta A \qquad 2\text{-}7$$

Here, equation 2-4 is equal to equation 2-7 for the three different types of frictional/drag force, and by substituting the different frictional/drag force types in the integral we will have a relation between the change in amplitude (loss in amplitude ΔA) and the amplitude of oscillations.

a) Velocity- independent frictional force ($F_r = f_0\hat{v}$)

Let's start by substituting the force into the integral in equation 2-4:

$$\Delta E = \int_0^T f_0 . L\hat{\dot{\theta}}\, dt \qquad 2\text{-}8$$

$$\Delta E = f_0 L \int_0^T [-\omega A \sin(\frac{2\pi}{T} t)]dt \qquad 2\text{-}9$$

By integrating it over a complete period ($0 \rightarrow T$ or $t \rightarrow t + T$),

$$\Delta E = 4Lf_o A \qquad 2\text{-}10$$

This is equal to equation 2-7.

$$\Delta E = 4Lf_o A = m\omega^2 A\, \Delta A \qquad 2\text{-}11$$

So, there is a constant relationship between the change in amplitude (loss in amplitude ΔA) and the amplitude of oscillations in the case of velocity-independent frictional force (i.e. ΔA is simply a constant and is independent of A).

$$\Delta A = \frac{4L\, f_o}{m\omega^2} = \frac{Lf_o T^2}{\pi^2 m} \qquad 2\text{-}12$$

This type of frictional force should give decaying oscillations represented by a cosine wave with an envelope of a straight line such that the drop in amplitude is constant between any two consecutive cycles.

b) Viscous (linear) drag force ($F_r = f_1 v\hat{v}$)

Substituting this force into the integral in equation 2-4 now gives:

$$\Delta E = \int_0^T f_1 . L^2 \dot{\theta}\hat{\theta}\, dt \qquad 2\text{-}13$$

$$\Delta E = f_1 L^2 \int_0^T [-\omega^2 A^2(t) \sin^2(\frac{2\pi}{T} t)\ ]\quad dt \qquad 2\text{-}14$$

By integrating it over a complete period ($0 \rightarrow T$ or $t \rightarrow t + T$),

$$\Delta E = \pi L^2 f_1 \omega A^2 \qquad 2\text{-}15$$

This is equal to equation 2-7.

$$\Delta E = \pi L^2 f_1 \omega A^2 = m\omega^2 A\, \Delta A \qquad 2\text{-}16$$

So, there is a linear relationship between ΔA and A in the case of viscous drag force.

$$\Delta A = \frac{\pi L^2 f_1}{m\omega} A = \frac{L^2 f_1 T}{4\pi m} A \qquad 2\text{-}17$$

This force was the same drag force in equation 1-4. So, for, $f_1 = a\,\eta$, the loss in amplitude (ΔA) is directly proportional to the viscosity of the medium.

$$\Delta A = \frac{a\,\eta\, L^2 T}{4\pi m} A \qquad 2\text{-}18$$

This behavior is in agreement with the solution obtained by solving the differential equation directly, which gives an exponential decay of the amplitude of the oscillations with time.

c) Inertial (quadratic) drag force ($F_r = f_2 v^2 \hat{v}$)

In this case one gets:

$$\Delta E = \int_0^T f_2 . L^3 \dot{\theta}^2 \hat{\theta}\, dt \qquad 2\text{-}19$$

$$\Delta E = f_2 L^3 \int_0^T [-\omega^3 A^3(t) \sin^3(\frac{2\pi}{T} t)\ ]\ \ dt \qquad 2\text{-}20$$

By integrating it over a complete period ($0 \rightarrow T\ or\ t \rightarrow t + T$),

$$\Delta E = \frac{8}{3} L^3 f_2 \omega^2 A^3 \qquad 2\text{-}21$$

This is equal to equation 2-7.

$$\Delta E = \frac{8}{3} L^3 f_2 \omega^2 A^3 = m\omega^2 A\, \Delta A \qquad 2\text{-}22$$

So, there is a quadratic relationship between ΔA and A in this case of an inertial drag force.

$$\Delta A = \frac{8L^3 f_2}{3m} A^2 \qquad 2\text{-}23$$

This force was the same drag force in equation 1-5. Thus, $f_2 = \frac{C_D S}{2}\rho$.

$$\Delta A = \frac{8L^3 C_D S\, \rho}{6m} A^2 \qquad 2\text{-}24$$

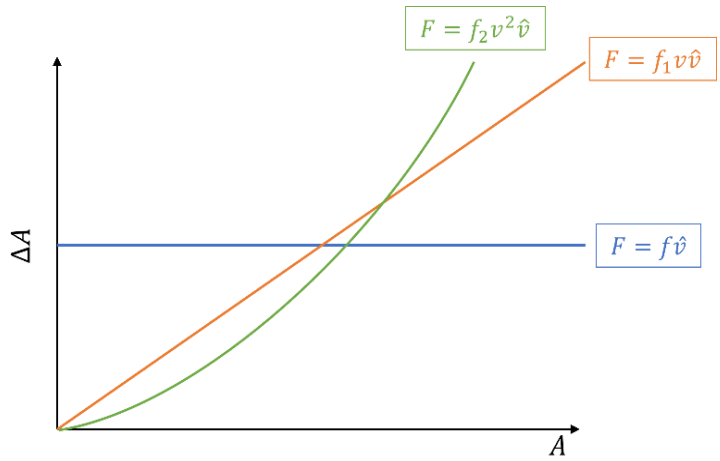

Figure 2.2: The change in amplitude as a function of the amplitude, which is equivalent to the energy loss curves for various drag forces.

So, the energy loss curve (or more specifically $\Delta A\ vs. A$ curve) clearly depends on the nature of the frictional/drag force at play in the pendulum system. Figure 2.2 shows the general behavior of $\Delta A\ vs. A$ for the three different drag force types.

So far, we studied the decay of the amplitude of the oscillations for each type of drag force separately. Yet, this powerful method in analysing the damping mechanism of the physical pendulum allows the study of real problems where all three damping mechanisms might be present. The $\Delta A\ vs. A$ curve can then be analysed using a polynomial fit $\Delta A = aA^2 + bA + c$, where $a,\ b, and\ c$ are the fit constants equal to the constants in equations 2-22, 2-17, and 2-12 respectively.

2.2 Differential-Equation-Based Analysis

In the case of the highly laminar regime, the relation between $\Delta A\ and\ A$ -or between the drag force and the velocity- is linear. Neglecting both the inertial drag force (i.e. $\gamma_2 \to 0$) and the constant frictional force on the fulcrum (i.e. $f_0 \to 0$). Then equation 2-3 becomes,

$$\ddot{\theta} + 2\gamma_1\,\dot{\theta} + \omega_0\theta = 0 \qquad \textit{2-25}$$

This equation is directly solvable using the analytical differential-equations-based methods, with the following general solution for $\theta(t)$.

$$\theta(t) = e^{-\gamma_1 t}(A_1 e^{\sqrt{\gamma_1^2-\omega_0^2}t} + A_2 e^{-\sqrt{\gamma_1^2-\omega_0^2}t}) \qquad \textit{2-26}$$

Where A_1 and A_2 are constants.

This solution is divided into three different regimes: the critical damping regime when $\gamma_1^2 = \omega_0^2$, the over damping regime ($\gamma_1^2 > \omega_0^2$), and the under damping regime ($\gamma_1^2 < \omega_0^2$). The pendulum reaches the equilibrium position (i.e. theta equals zero) without oscillating around it when one of the first two conditions is satisfied. In

critical damping, the pendulum moves toward the equilibrium faster than in the over damping (Pain 2005).

Yet, in the third case (under damping), the damping causes the pendulum to return to equilibrium with an oscillating amplitude that decreases until it reaches zero eventually. These oscillations have an angular frequency of $\omega'^2 = \omega_0^2 - \gamma_1^2$. Applying the under damping condition on equation 2-26, the general solution will be (Pain 2005):

$$\theta(t) = A\, e^{-\gamma_1 t}\, cos\, cos\, (\omega' t + \phi) \qquad 2\text{-}27$$

Where A is a constant and ϕ is a phase shift.

where γ_1 is directly proportional to f_1 (i.e. to η) and to the length of the pendulum (L_{CM}), while inversely proportional to the moment of inertia (I). So, we can calculate the viscosity of the liquid using the equation 2-27 only if the motion is in the highly laminar regime (i.e. $Re < 1$).

$$\gamma_1 = \frac{a\eta\, L_{CM}}{2I} \qquad 2\text{-}28$$

2.3 Period of Oscillation as a Function of Viscosity

The damping constant depends directly on the viscosity when the motion exists in the highly laminar regime (Hou, et al. 2015), as mentioned before. Consequently, the angular frequency of the oscillations (ω'^2) changes with the viscosity, and so the period of oscillations.

$$\frac{2\pi}{T} = \sqrt{\left(\frac{mgL_{CM}}{I}\right)^2 - \left(\frac{a\eta L_{CM}}{2I}\right)^2} \qquad \textit{2-29}$$

Substituting $I = \frac{1}{3}mL_{CM}^2$, the period of oscillation becomes:

$$T = \frac{4\pi m L_{CM}}{\sqrt{(2mg)^2 - (a\eta)^2}} \qquad \textit{2-30}$$

To further process this function, the denominator will be expanded by the Taylor series expansion of the second order

$$\sqrt{(2mg)^2 - (a\eta)^2} = \sqrt{(2mg)^2} - \frac{a^2\eta^2}{\sqrt{(2mg)^2}} + O(\eta^4) \qquad \textit{2-31}$$

$$\sqrt{(2mg)^2 - (a\eta)^2} \cong 8(mg)^2 - a^2\eta^2 \qquad \textit{2-32}$$

And thus, the period equals

$$T = \frac{4\pi m L_{CM}}{8(mg)^2 - a^2\eta^2} \qquad \textit{2-33}$$

3 Experimental Setup and Methodology

We developed and fabricated a unique new design of a physical pendulum that is specialized to be used as a viscometer. Its design allows it to be used for a huge range of viscosities and gives excellent sensitivity. Here, we will describe this new design and contrast it with existing pendulum viscometers from the literature.

3.1 Design

Pendulums have been used to measure the viscosity, as mentioned before. It has been long observed- since the middle ages that liquids' viscosity and density affect the damping of different pendulum types when immersed in the liquids. But, all of these new and old versions of the pendulum viscometers have been dependent on immersing all of the pendulum or the end part of it in the liquid whether it was a physical (Janik, et al. 2006), simple (Zonetti, et al. 1999, Leme and Oliveira 2017), or torsion pendulum (Hong and Lu 1995) (Figure 3.1 A). This approach limited such studies in the literature to very small angles and velocities to record the pendulum oscillations at Reynolds numbers smaller than 1, so they neglect the inertial drag force. Thus, the equation could be solved with the viscous drag force only being considered, and gave a direct linear relationship between the damping constant and the viscosity of the liquid. Furthermore, these previous designs were restricted in terms of the viscosity of the liquid since the oscillations die quickly when the pendulum is immersed in liquids with significantly higher viscosities than water (e.g. higher by 100 times or more than water). This limited the types of liquids that can be studied using the technique and thus limited the significance of the instrument as a viscometer. Furthermore, the relatively short length of the pendulum arm

-needed to keep its mass small- limits the angle/oscillation amplitudes that can be resolved reliably. We devised and used a new pendulum design that resolves both of the previous problems and significantly improves the versatility of the pendulum as a viscometer. Our physical pendulum viscometer design is shown in Figure 3.1B), where the main idea of this design is to attach the part (or mass) that will be immersed much closer to the upper part or suspension point of the pendulum. This was done by attaching a small bar at 90 degrees to the pendulum rod with two arms at its ends each with a small ball "sphere" suspended from it and moving parallel to the pendulum. The component parallel to the pendulum rod of the distance between the sphere and the fulcrum point is (l). This distance is significantly less than the

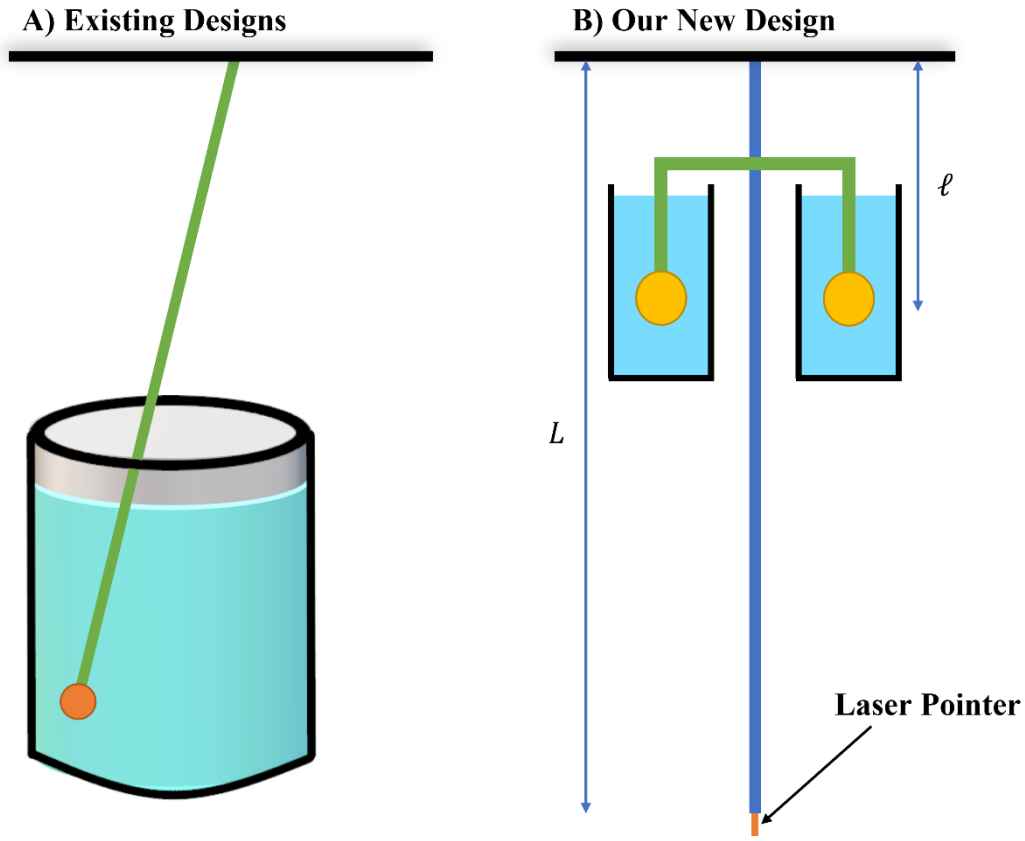

Figure 3.1: Pendulum viscometer A) Old designs. B) Our new design for the physical pendulum viscometer, where L is the total pendulum's length, and ℓ is the distance from the center of the fulcrum point to the center of the oscillating spheres.

length of the pendulum rod (L), so the velocity of the sphere is significantly less than the tip of the pendulum for a given oscillation amplitude (i.e. $\ell \times \dot{\theta} \ll L \times \dot{\theta}$). A second major improvement to the design is attaching a small laser to its end, reflecting the laser beam from a mirror placed at 45 degrees on a wall. This gave us an 'effective length of a few meters of the pendulum arm'.

So, the new pendulum viscometer has multiple major improvements and capabilities, like:

1- having $\ell \ll L$ enables us to study the oscillations at larger angles and in liquids with higher viscosities while still having a small Reynolds number (equation 1-3) since we have reduced the velocity of the immersed parts of the pendulum in the liquid. The velocity of each moving sphere equals:

$$v_{sphere} = \frac{\ell}{L}\, v_{Pendulum} \qquad 3\text{-}1$$

In which $v_{sphere} = \ell\, \dot{\theta}$ is the velocity of the moving ball, $v_{pendulum} = L\, \dot{\theta}$ is the velocity of the tip of the pendulum, ℓ is the distance from the fulcrum point to the center of the ball, and L is the length of the whole pendulum's arm. Consequently, the Reynolds number is reduced by the same factor.

2- For a given liquid, the torque acting due to the drag force on the two spheres is significantly smaller than one gets if the tip of the pendulum arm was in the liquid. This allows us to study fluids with extremely high viscosity and non-Newtonian fluids.

3- The very light weight of the thin (5.59 mm diameter), hollow aluminum cylinder comprising the rod of the pendulum makes it extremely sensitive to small drag forces/viscosities. Yet, more importantly, the sensitivity can be tuned by attaching weights close to the tip of the pendulum to increase the moment of inertia and make the torque of the returning force (i.e. $msin\,(\theta)$) stronger compared to that due to the viscous drag force at distance (ℓ). So, removing any extra weights reduces the moment of inertia of the pendulum to a minimum and makes it extremely sensitive to low viscosities. This comes at the cost of losing the ability to measure highly viscous fluids, yet attaching a weight to the pendulum reduces the sensitivity and allows the study of very viscous liquids.

4- Attaching the immersed masses closer to the suspension point of the pendulum does not affect the symmetry of the viscometer. Where suspending two spheres on the right and left sides of the attached small bar keeps the symmetry in our design.

5- The crucial addition of the laser pointer to the end of the pendulum enhances the sensitivity significantly, where even minute oscillations cause the bright spot on the wall to move by an amount easily picked by the camera and the 'Tracker' software.

6- In addition to that, our new physical pendulum viscometer design has other features, such as the ability to apply an external magnetic field to easily study the magneto-viscous effects in magnetorheological fluids and ferrofluids using our setup.

7- Finally, even more flexibility is allowed by changing some of the pendulum parameters like the distance between the fulcrum point and the center of the spheres l, the mass suspended to the pendulum, and the diameter of the immersed spheres,

all of which can be changed to tune the device to a specific viscosity range of interest.

3.1.1 Technical Details

Through the initial months of working in developing and fabricating this physical pendulum viscometer design, the setup has been developed in many stages. Initially, we started working with a rectangular aluminum arm with a length of 44.5 cm, a width of 2.5 cm, a thickness of 3 mm, and a mass of 90 grams. The ball bearing was used as a fulcrum in this system. But, the pendulum's oscillations were linearly and rapidly damped with no noticeable difference between the dry (air only) damping and in-water damping. This clearly indicated that the friction at the suspension point dominated the damping mechanism leaving the pendulum insensitive to viscous drag in liquids. In order to fix this problem, we first changed the arm into a hollow aluminum rod with a length of 45.3 cm, a diameter of 5.95 mm, and a mass of 33 grams. Also in this case the ball bearing was used as a fulcrum. Even though the difference became more clearly noticed when comparing the dry damping and on-water damping, the pendulum oscillations were still linearly damped. At that moment, we considered that the hollow rod is a great choice for the arm but we have to change the method of suspending the pendulum. So, we used a hook screw as a fulcrum. In this version of the setup, the hook screw was attached to the aluminum rod and suspended on a cylindrical horizontal shaft. This choice was finally adopted for our research since it gave extremely small friction torque on the fulcrum, which turned out to be much less than the viscous drag torque. This suspension method makes only one contact point -with a fairly small

contact area- with the suspension shaft, the distance between the point of contact and the true axis of rotation (R) is extremely small. This distance is equal to the radius of the suspension shaft. So, ultimately the frictional torque ($\tau_r = f_r R$, where

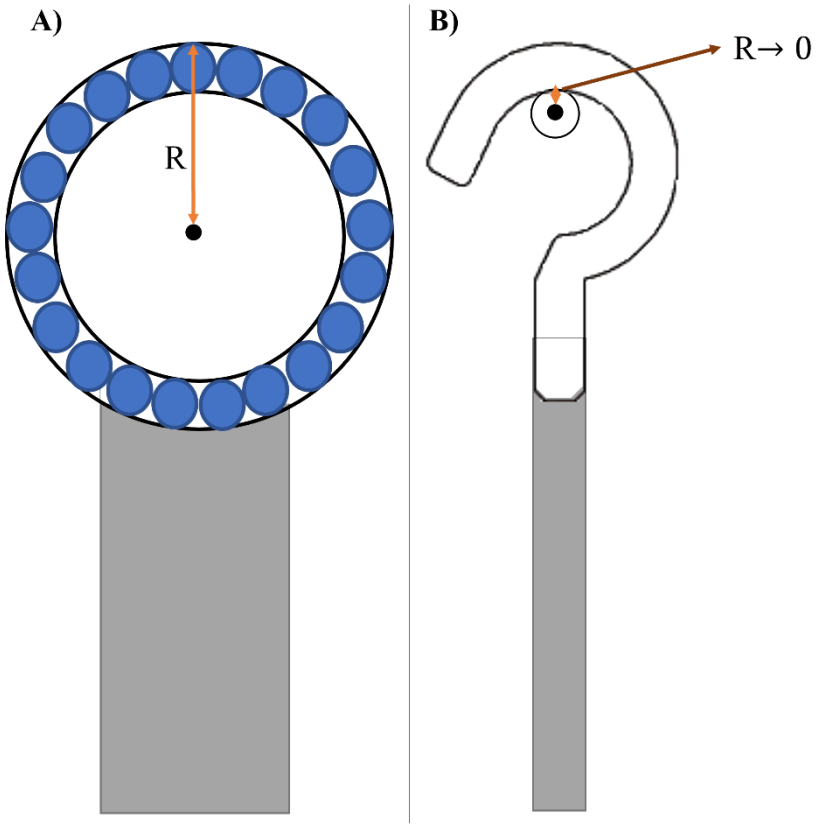

Figure 3.2: Sketch of the different fulcrum methods used A) Ball bearing fulcrum B) Hook screw fulcrum. Clarify how the radius of rotation differs between the two cases and so the frictional torque.

f_r is the frictional force and R is the radius of the rotation axis) goes to zero. In the case of ball bearing fulcrum, the contact with the shaft was larger -due to the multiple bearings- leading to larger values of 'moment arm' (τ_r) and the radius of the shaft (R) was much larger, so the actual friction torque was too large as shown in Figure 3.2. The placement of the bearings was extremely delicate and added significantly to the resistance due to misalignment and due to the cavity for the bearings being too narrow or too wide.

A rectangular aluminum (Al) support piece (shown in green) was attached using hot silicon on the Al rod as shown in Figure 3.3. Its distance from the suspension points is about 5 cm. This piece has c two thin copper (Cu) wires; one connected on each side of it such that they are parallel to the main pendulum rod. The length of each of them is (4.5 ± 0.1) cm and a plastic sphere with a diameter (d) of (9.55 ± 0.01)mm and a mass (m) of (0.47 ± 0.01) $grams$ was attached to the end of each wire. These two spheres oscillate parallel to the the pendulum's tip at a distance (ℓ) of (9.9 ± 0.1) cm from the center of the fulcrum point. Two plastic boxes were 3D-printed and have a length of 79 mm, a width of 23 mm, and a height of 31 mm. These boxes will be filled with the different liquids and placed on a fixed table (blue surface in Figure 3.3) such that the small spheres will oscillate inside the liquid and will thus be used to measure the liquid's viscosity. The final physical pendulum viscometer used in this thesis has a total length (L) of (50.9 ± 0.1) cm. This length increases significantly when counting the laser's path length to the wall, as will be discussed below. The total mass (M) of the moving parts of pendulum

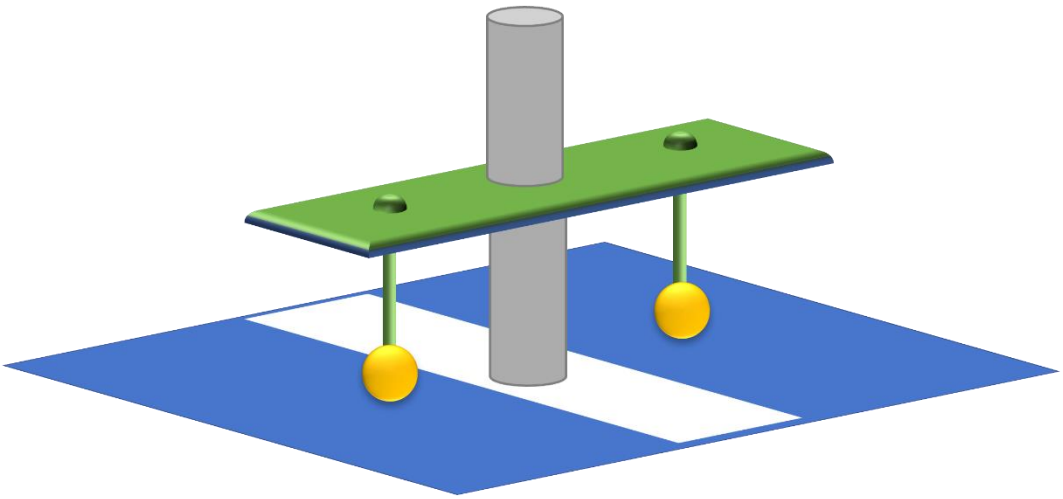

Figure 3.3: Sectional sketch of the physical pendulum viscometer for the rectangular piece and the suspended spheres.

was (38.3855 ± 0.0001) grams. That included the mass of the Al rod, the hook screw suspension, the support Al piece, the Cu thin wires, the spheres, and the laser pointer.

3.2 Data Collection and Analysis Methods

To monitor the physical pendulum's oscillations with the best resolution (i.e. angular precision), a laser pointer was suspended from the end of the pendulum's arm and aligned parallel to the arm. The laser beam falls on a mirror tilted at 45 degrees, which reflects the laser beam into a screen at a distance of 364 cm from the tip of the pendulum's arm as shown in Figure 3.4. This gives an effective length (L_{Laser}) of 364 cm added to the length of the pendulum (L). Thus, we are able to detect the fine oscillations, where the bright spot still moves even when the pendulum oscillations are hardly observed with the naked eye. Furthermore, this effective length is flexible and can easily be increased to give higher sensitivity. Yet, this increase

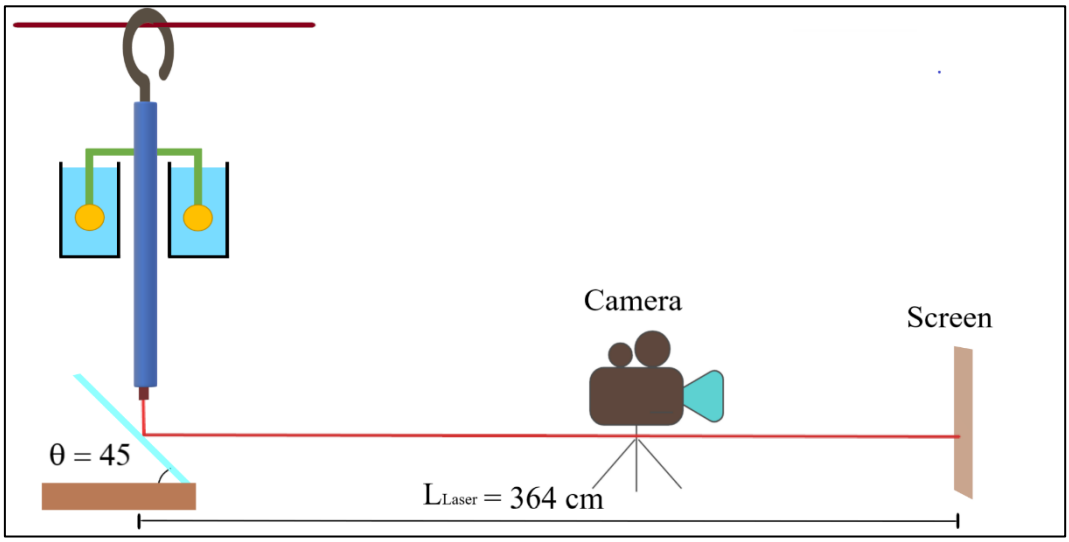

Figure 3.4: Sketch of the complete setup with clarifying the monitoring and data collection method. Where a laser pointer is aligned vertically with the pendulum's arm and reflects the beam from 45° tilted mirror on a screen apart of 364 cm.

in distance comes at the cost of making the laser spot get enlarged significantly. A better-quality laser pointer is recommended -if available- for this setup.

The laser bright spot moved/oscillated on the screen/wall giving significantly amplified oscillations of the pendulum. The oscillating bright laser spot was monitored with a (CANON or what make and model camera) camera capable of recording videos at a wide range of speed. We captured the videos at a speed of 250 frames per second. This system was built in order to get a better resolution in monitoring the angular position of our physical pendulum viscometer, where the larger length increases the angular resolution and precision.

$$\theta = \left(\frac{x}{L+L_{Laser}}\right) \cong \frac{x}{L+L_{Laser}} \qquad 3\text{-}2$$

Where θ is the angular position, x is the horizontal position of the laser point, L is the pendulum's arm length, and L_{Laser} is the distance between the screen and the center of the pendulum's arm. This system gives an angular resolution of about 2×10^{-5} radians (i.e. about 0.001 degrees).

3.2.1 Tracker Software

The captured videos were analyzed using the "Tracker Video Analysis Software" (Brown 2008, Brown and Cox 2009). The Tracker software is an accurate tool that analyzes the videos by tracking the different features as needed by the user. It is developed and built on the "Open-Source Physics" platform and is a user-friendly software that can be downloaded from the internet (https://physlets.org/tracker/) and runs on different operating systems.

In this project, the Tracker was used to track the laser point on the screen and to determine its horizontal position (x) through the pendulum's oscillations, with tracking the oscillating time. Figure 3.5 shows a snapshot of the Tracker software screen while it was analyzing one of the captured videos. On the left side, It shows the inserted video with 4 different blue lines which were the calibration sticks to convert/ calibrate the pixels of the camera into real distance units, with the coordinate axis in pink to determine the zero-point. On the right side, it shows the resultant curve of the horizontal displacement of the bright point as a function of time with a table records the numerical data points of the horizontal and vertical displacements with the time.

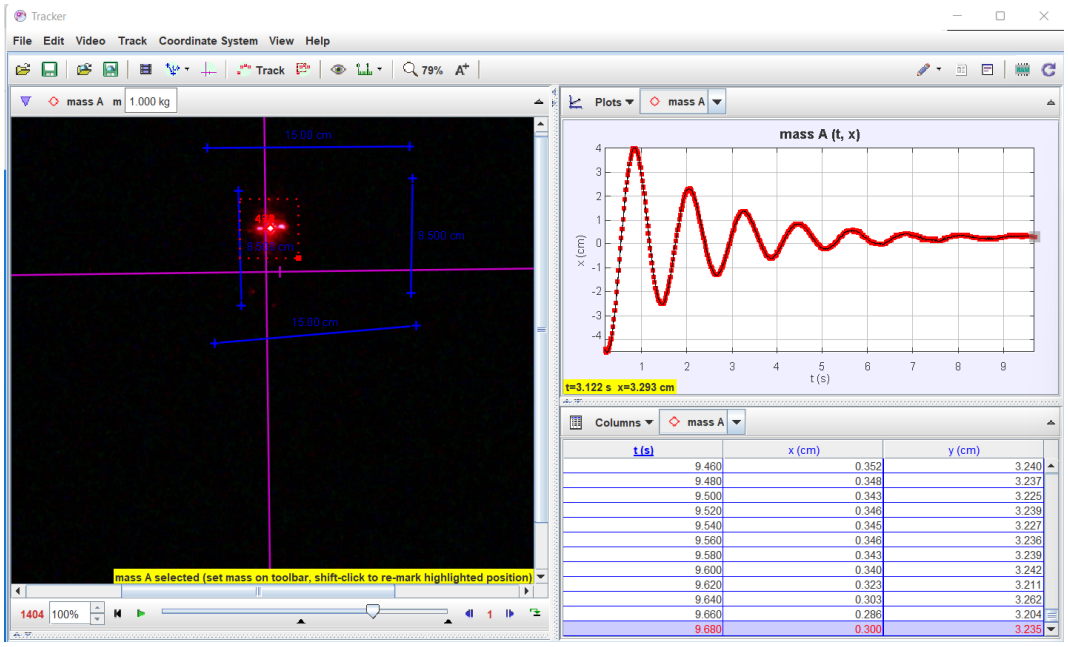

Figure 3.5:A snapshot of the "Tracker Video Analysis Software" screen while it analyzes a video.

3.2.2 LabVIEW

The “Laboratory Instrument Engineering Workbench” or the LabVIEW is a visual programming language/system that was developed by the “National Instruments” (NI) in the early 1980s. It is an easy graphical programming language that can be used for Data Acquisition (DAQ) purposes, tests, measurements, and the different analysis processes (Andrade and Kovner 1998, Johnson and Jennings 2006, Travis and Kring 2007).

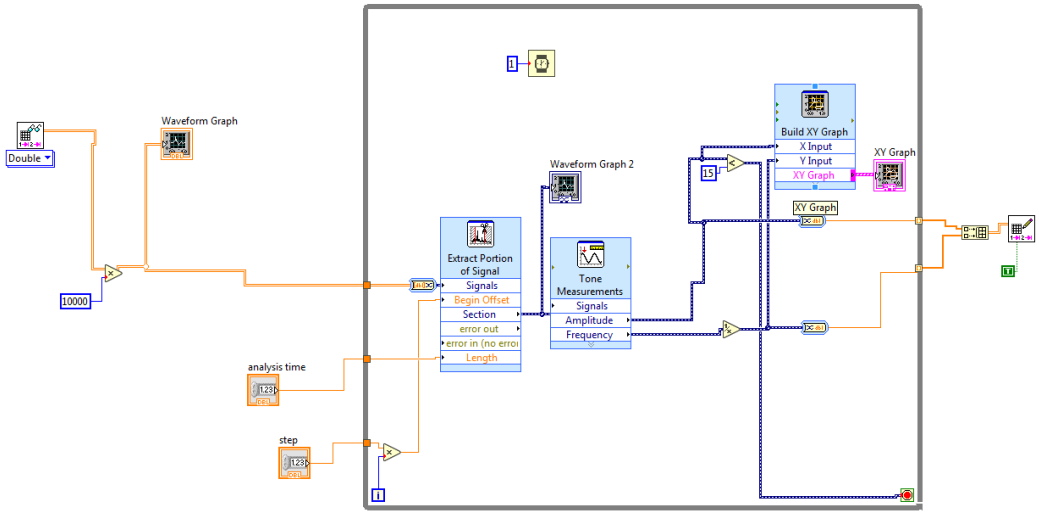

Figure 3.6: A snapshot of the "LabView Program" block diagram screen (See Appendix B for more clarification).

In this thesis research, we used LabVIEW to read/analyze Tracker-generated data and record the amplitudes and the period of oscillations. The data taken from ‘Tracker’ software is modified on Excel sheets to give the pendulum’s angular displacement (θ) as a function of oscillations’ time (by dividing the horizontal displacement points over the summation of the length of the pendulum and the laser’s effective length), then saved into a text file with the format MS-DOS. This file was

then read by LabVIEW and processed, where the ‘extract portion of signal’ function in a LabView program (shown in figure 3.6 or Appendix B) was used -with an analysis time equal to 600 and a step of 20 data points- to extract (or read) a small portion of the θ(t) file in order to find the average amplitude and period of the oscillation within this small-time window. The last two numbers are related to the size of the window of analysis used in this function and the step to determine the next window in extracting the average amplitude and period. The amplitudes and period of oscillations were then measured by the next LabVIEW function ‘tone measurements’, which takes the extracted data within the small window and calculates the amplitude, the frequency (i.e. the period of oscillations), and the phase for a signal tone. The processed data was finally saved as a matrix of two columns (the amplitude and the period) on a text file. Figure 3.6 shows a snapshot of the ‘Block Diagram’ (the actual LabVIEW program) we used in reading and analysing pendulum motion videos for finding the amplitudes and periods of oscillations in this thesis. The LabVIEW program is a simple and powerful technique to automate the entire video analysis process and extract vital information about the motion.

3.3 Capillary Viscometer

We used two ways to verify/evaluate the performance of our new physical pendulum viscometer and to calibrate it:

a) comparison with viscosity data from the literature, and
b) Using the well-known capillary viscometer (Viswanath 2007) to measure all liquids with it and compare the results with those obtained by the pendulum viscometer. The principle of the capillary viscometer is to

determine the flow time of the liquid through the capillary tube or a tube of a very small diameter. Since the flow of a liquid through a vertical tube is retarded by the viscosity, its flow time will depend on the viscosity (η) and the density (ρ). The more viscous liquids will have a longer flow time, while the more dense liquids will have a shorter flow time. Thus, there is a direct proportionality between the flow time and viscosity but an inverse proportionality between the flow time and the density.

$$\eta = t \times \rho \qquad 3\text{-}3$$

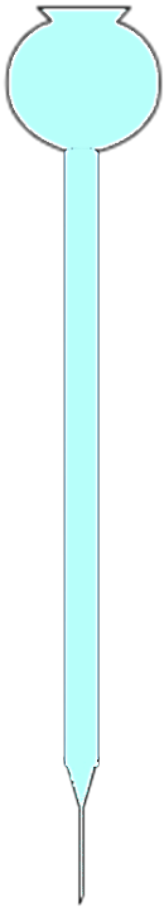

Figure 3.7:Sketch of the capillary tube viscometer used in this project; this viscometer has been fabricated in the Glass department in the Chemistry laboratories.

In this project, the viscosity was measured relative to water by measuring the flow time for the liquids between two determined points on the vertical tube. Figure 3.7 shows a sketch of the used capillary tube viscometer, this viscometer has been fabricated in the Glass department in the Chemistry laboratories at Birzeit University.

3.4 Studied Liquids

I studied nine different liquids in this thesis, with their viscosities ranging from 1 mPa.s to 474 mPa.s. These liquids were Water, Ethylene Glycol with a concentration of 100%, Paraffin oil, and different motor oils which were, from the lighter to the heavier/more viscous, SAE 10W, SAE 0W-20, SAE 5W-30, SAE 5W-40, SAE 15W-40, and SAE 10W-60.

4 Data And Analysis

4.1 Pendulum oscillations damping in different liquids

Details of the periodic oscillations of a pendulum depend on the frictional\drag forces acting on it, as mentioned before. Since our physical pendulum design has been fabricated with an extremely small fulcrum friction force, we can see that the linear damping term (velocity independent frictional force term) in equation 2.3 mostly disappears even in the dry damping (in-air damping) case as shown in Figure 4.1. Figure 4.1 A) shows the complete dry oscillations of our physical pendulum when it starts oscillating from an angle of o.21 degrees. These oscillations took a total time of about 600 seconds (10 minutes) to rest after about 480 periods with a

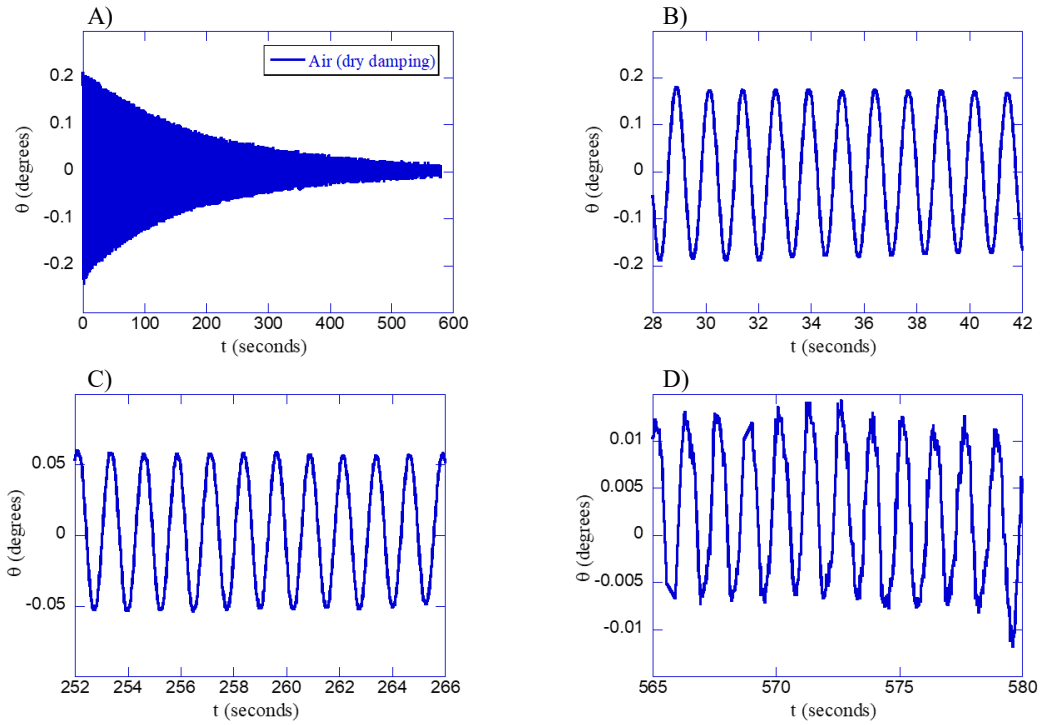

Figure 4.1: Graphical output of our physical pendulum viscometer oscillations as a function of time (angles smaller than 0.3 degrees), while it is not immersed in any liquid (dry damping). A) The entire oscillation process until no more motion was detected, and three zoomed-in periods: B) t=28-42 s, C) t=252-266 s, and D) t=565-580 s.

period time of 1.25 seconds. Further, the data shows a clear exponential decay/ damping, which confirms that the linear damping term was dominant and that both the frictional torque acting on the fulcrum and the quadratic drag force were approximately equal to zero. Additionally, Figures 4.1 B) and C) show zoomed-in areas of the oscillations of 4.1 A) at different intervals: at the beginning and in the middle of the oscillations time. It is visible that we have very clear and periodic oscillations. In addition, Figure 4.1 D) shows the oscillations towards the end (i.e. at very small angles). Even though there are some fluctuations that appeared in this interval –presumably due to very small oscillations at the fulcrum point in directions different from the main pendulum motion-, it still has clear and well-resolved periodic oscillations. After immersing the two upper arms and the spheres (recall Figure 3.1B) in the water we observed that the oscillations took about half the time to die out compared with the dry damping case. As shown in Figure 4.2 A) these oscillations are still long where the complete oscillations took about 300 seconds (5 minutes) to finally reach to rest. This took about 240 periods with a period time of 1.26 seconds when the initial oscillations started with an amplitude/angle of 0.24 degrees. Figures 4.2 B), C), and D) show a zoom-in of Figure 4.2 A) at different intervals: the beginning, the middle, and towards the end of the oscillations. As in the dry damping case, even though there are fluctuations at very small angles (close to the end), yet the periodic oscillations are still quite obvious and clearly resolved. It is important to also notice here that we have clear and complete oscillations with an amplitude of 0.001 to 0.002 degrees (2 to 3 $x10^{-5}$ radians)!

In spite of these fluctuations, the hook-screw-based fabrication was the best fabricated physical pendulum for our viscometer: Its oscillations lasted long enough to allow us to reliably measure the viscosity of both lighter liquids such as water and significantly heavier, more viscous liquids.

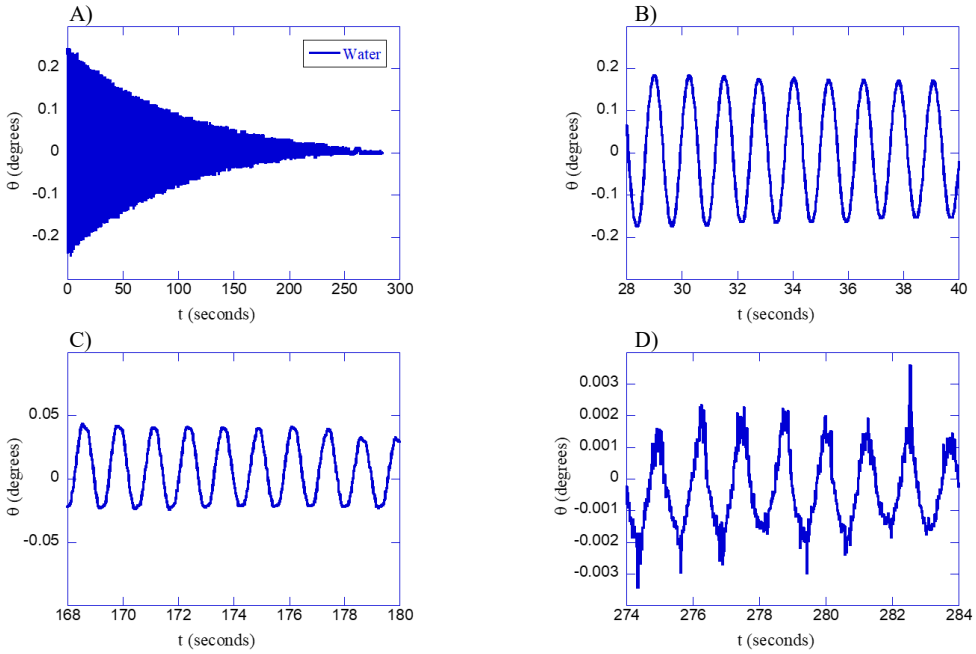

Figure 4.2: Graphical output of our physical pendulum viscometer oscillations as a function of time (angles smaller than 0.3 degrees), while it was immersed in water. A) total oscillations time, and zoom-ins B) $t = 28 - 40$ *, C)* $t = 168 - 180$*, and D)* $t = 274 - 284$ *seconds*

Earlier models of the pendulum viscometer had important flaws/drawbacks: A similar pendulum -but with ball-bearings-based suspension as a fulcrum point- had significantly higher friction. This is further amplified by multiplying it by a larger 'moment arm' (recall Figure 3.2B) giving a significant frictional torque that dominated the damping behaviour of the pendulum. Figure 4.3 shows the oscillations of this initially fabricated physical pendulum viscometer. Its oscillations even in air

(dry damping) came to rest after less than 10 seconds when it started oscillating from an angle of 0.29 degrees. So, the final design with the hook-screw-based physical pendulum took about 60 times longer to complete its oscillations and come to rest. Furthermore, it is easy to see that oscillation amplitude drops by the same amount after each cycle (i.e. there is linear envelope of the oscillations) indicative of a constant (i.e. velocity-independent) drag force usually taking place at the suspension point/fulcrum rather than in the damping liquid (Figure 4.3 A).

This constant damping causes the oscillation process to seize to exist abruptly (linearly) without giving the user an opportunity to observe the oscillation at small angles, as seen in Figure 4.3 B).

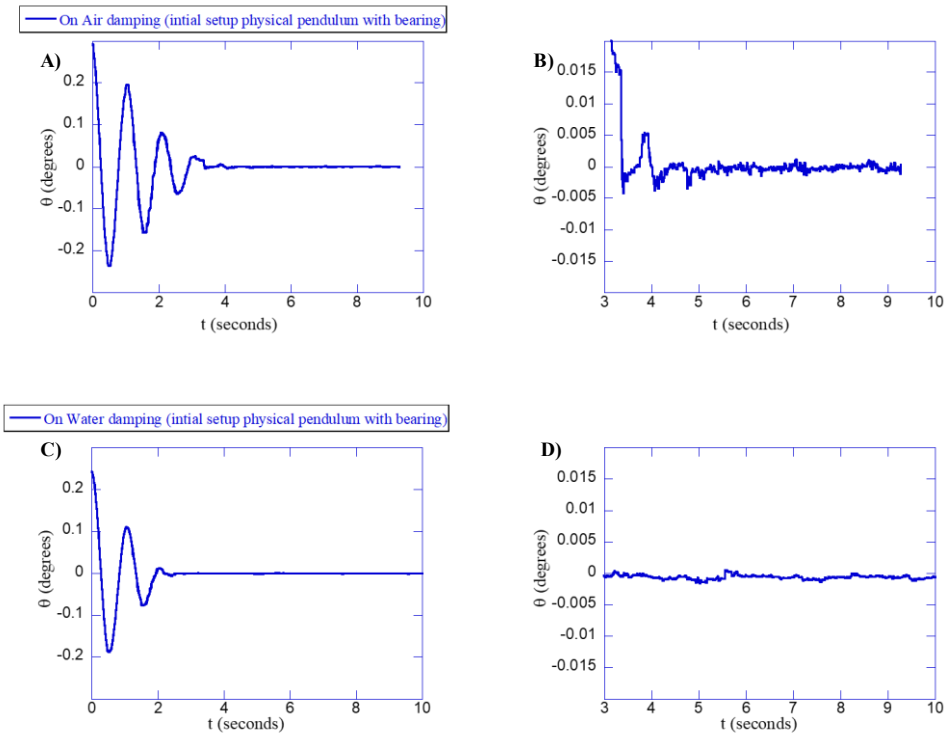

Figure 4.3: The graphical output of an initial setup of the physical pendulum viscometer oscillations as a function of time for a design depended on the bearing as a fulcrum point A) On air damping complete oscillations, B) On air damping with zoom in at the ends of oscillations, C) On water damping complete oscillations, and D) On water damping with zoom in at the ends of the oscillations.

In the case of water, as shown in Figure 4.3 C), the oscillations came to rest after about 5 seconds when starting with an initial oscillating angle of 0.24 degrees. The same linear behavior on damping was noticed with an obvious lack of oscillations at the very small angles (Figure 4.3 D).

As shown in Figure 4.4, we observed and studied the pendulum oscillations and damping while the upper arms and the spheres are immersed in eight different liquids that have viscosities ranging from that of water, about 20 times the viscosity of water -such as pure Ethylene glycol (Viswanath 2007, White 2009, Sawicka, Cieśliński and Smolen 2020) (Figure 4.4 A) where the pendulum oscillations continued for 90 seconds (1.5 minutes) when it starts oscillating from an angle of 0.26 degrees- to about 470 times the viscosity of water such as the viscous motor oil SAE 10W-60 (Zahariea and Husaru 2017) (Figure 4.4 H) where the pendulum oscillations continued for about 12 seconds when it starts oscillating from an angle of 0.24 degrees. Within these two values the studied liquids, as shown in Figure 4.4, were: B) Paraffin oil, C) motor oil SAE 10W, D) motor oil SAE 0W-20, E) motor oil SAE 5W-30, F) motor oil SAE 5W-40, and G) motor oil SAE 15W-40.

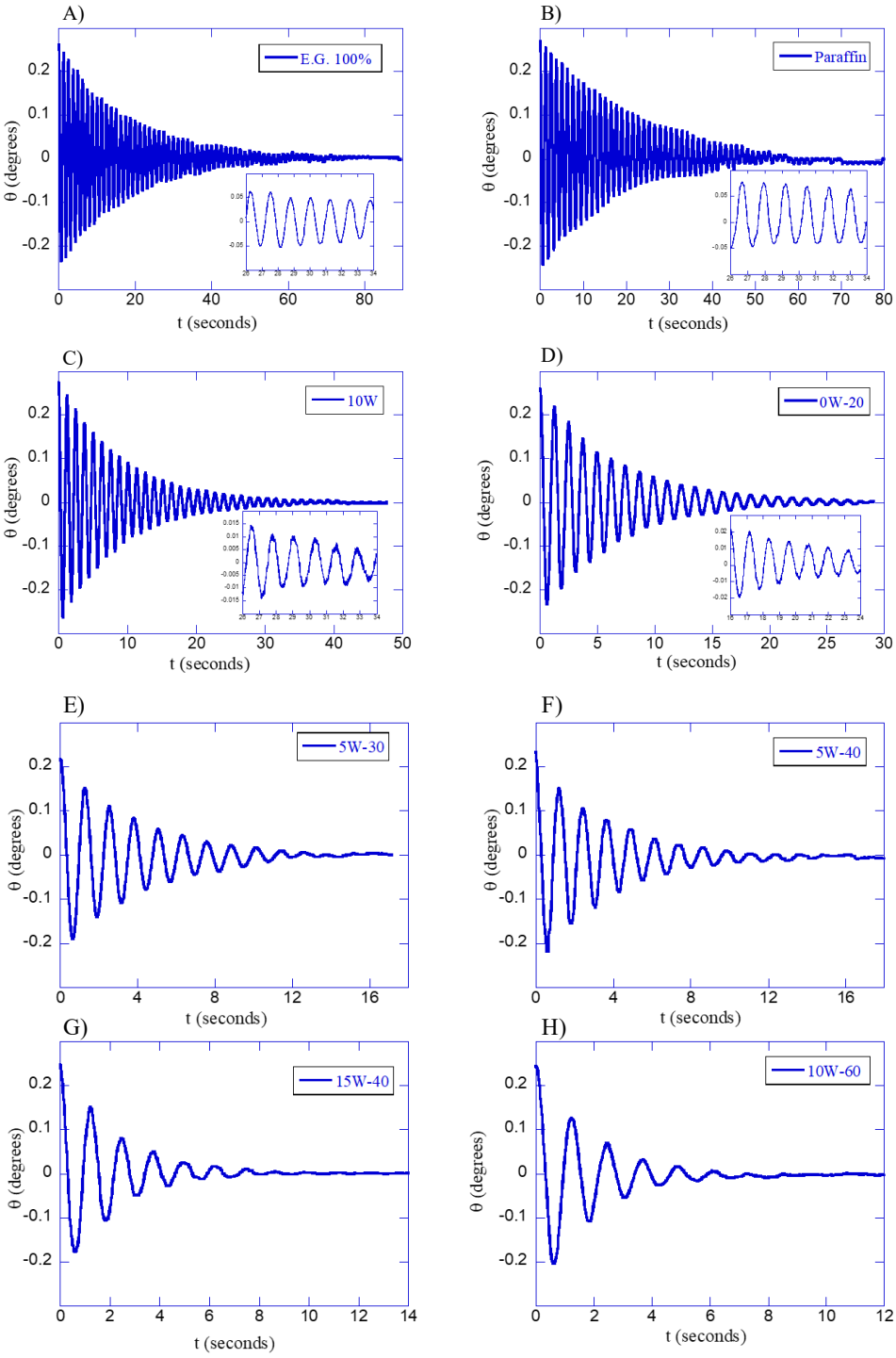

Figure 4.4 : Graphical output of our physical pendulum viscometer oscillations as a function of time (angles smaller than 0.3 degrees): viscous damping, immersed in A) pure ethylene glycol (E.G. 100%), and different types of light and viscous oils: B) Paraffin oil, C) SAE 10W, D) SAE 0W-20, E) SAE 5W-30, F) SAE 5W-40, G) SAE 15W-40, and H) SAE 10W-60.

Figure 4.5 shows a comparison of a small range of the oscillations in water -which is the lightest studied liquid-, the motor oil SAE 0W-20 which has an intermediate viscosity, and the motor oil which is the most viscous liquid. These curves are the same as in Figures 4.2, 4.4 D), and 4.4 H) respectively, but with a smaller time interval ranging from 0.8 seconds to 6.8 seconds to clearly demonstrate some differences between them. The decay in amplitude in the case of water is very slow while it becomes faster in the case of motor oil 0W-20 and very fast in the case of motor oil SAE 10W-60 (Figure 4.5 A). Furthermore, it can be seen that the period (T) increased with increasing the liquid's viscosity. These differences between the curves of the three liquids are more obvious when zooming in even further, as in Figure 4.5 B). One can also see that oscillations persist at very small angles. For instance, in the case of motor oil SAE 10W-60, we see two oscillations in this narrow time interval: The first with an amplitude of about 0.015 degrees and the second with an amplitude of about 0.005 degrees. Also, in the case of motor oil SAE 0W-20, we have two notable oscillations in this interval: the first with an amplitude of about 0.12 degrees and the second with an amplitude of about 0.1 degrees.

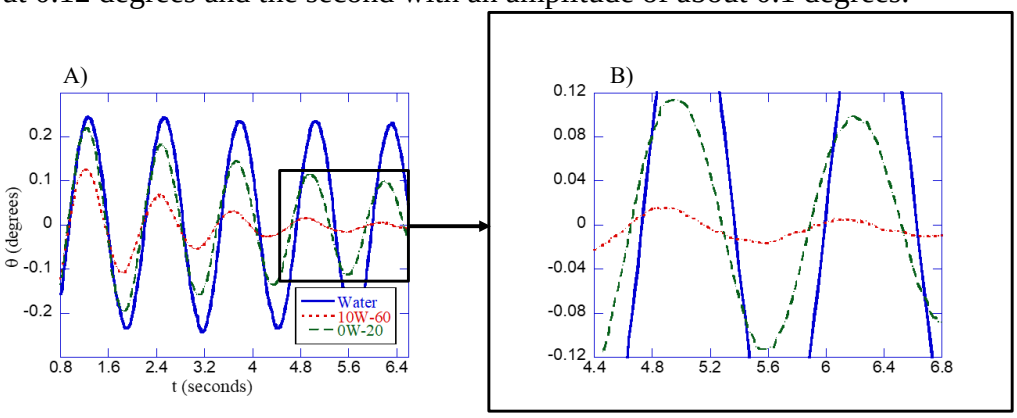

Figure 4.5: Graphical output of our physical pendulum viscometer oscillations as a function of time A) comparison of the pendulum oscillations while the spheres are immersed in three different liquids: water, 0W-20, and 10W-60. B) Zoom-in graph to display the oscillations at very small angles.

4.2 Energy-loss curves and the damping mechanism

We need to identify the energy loss behavior in order to study the damping mechanism of our physical pendulum and to identify the main drag forces/liquid viscosities acting on it. The behavior of the change in the oscillations' amplitude as a function of the amplitude itself ($\Delta A\ Vs.\ A$) gives a direct indication of the underlying energy-loss mechanisms.

Figure 4.6 shows the$\Delta A\ Vs.\ A$ relation., which looks linear, even though there are net vibrations in the data. These vibrations likely came from three different sources: 1) the conversion process of the videos to digital data and then extract values of the amplitude and period only in small stripes of time. 2) Our physical pendulum viscometer was very light, so it is very sensitive to any air vibration. 3) Unwanted oscillations and rotation of the pendulum suspension point, where the hook could also move perpendicular to the main motion. These fluctuations and small vibrations are invisible to the naked eye.

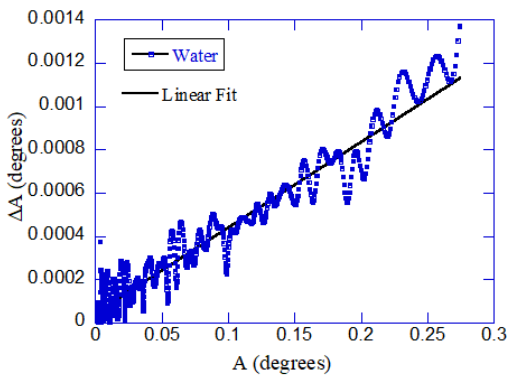

Figure 4.6: The change in oscillations amplitude ΔA as a function of the amplitude A, while the pendulum arms are immersed on water.

The LabView program that we wrote specifically for this purpose gave better results of the amplitude analysis than the Python program that came with the 'Tracker' software. The Python code (Appendix A) that was initially used to find the amplitudes of the oscillations gave significant scattering in the data besides the vibrations. On the other hand, the feature of averaging and analysis window in LabView helped reduce the scattering significantly, but did not eliminate it. Figure 4.7 shows a comparison between the outcomes of these two programs when used to analyse the same dataset of oscillations damped by immersing the spheres in water.

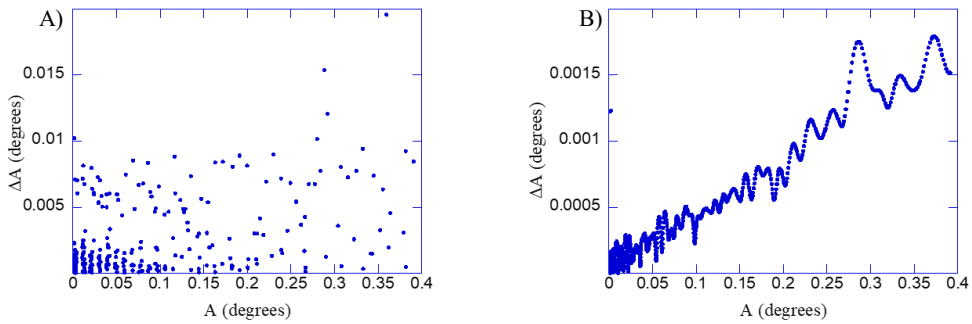

Figure 4.7: Comparison between the results of the change in oscillations amplitude ΔA as a function of the oscillations amplitude, while the pendulum arms are immersed on water. In the case of finding the amplitudes A) using simple Python code, and B) using simple LabView program.

Figure 4.8 displays four graphs of "$\Delta A\ Vs.\ A$" data; two of them obtained on the final pendulum design (hook-screw-based physical pendulum) while the other two obtained using an older design that relied on bearings for the suspension point. Figures 4.8 A) and C) clearly show the relation between ΔA and A to be purely linear and to have a y-intercept of about zero both in water and in air. The extremely low intercept demonstrates that the velocity-independent friction force at the fulcrum is

negligible, since the intercept is proportional to the velocity independent force (fulcrum frictional force) according to the equation:

$$y - intercept = \frac{\ell f_0 T^2}{\pi^2 m} \qquad 4\text{-}1$$

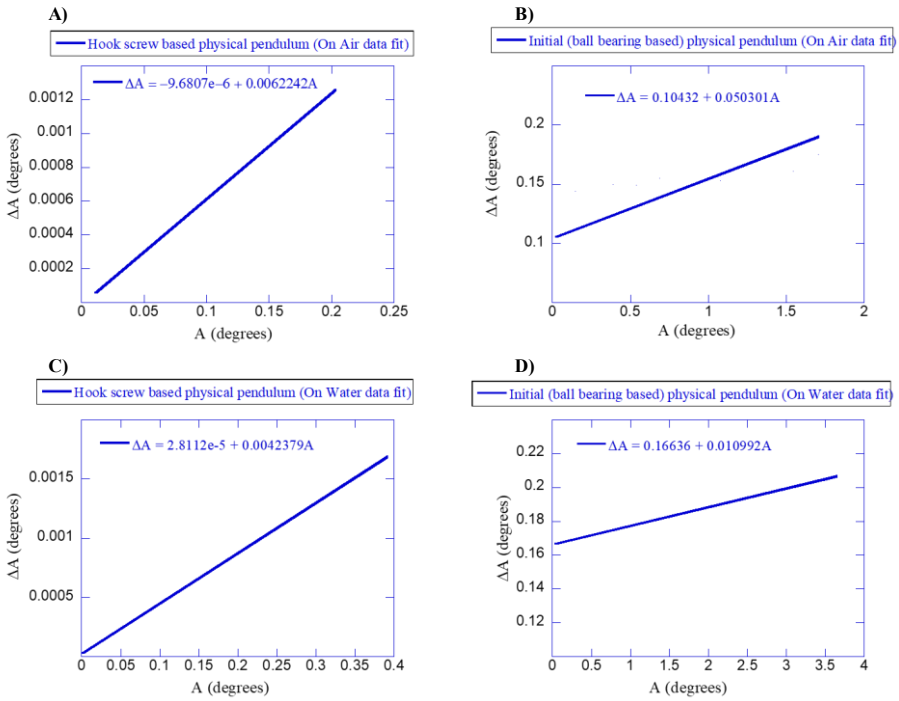

Figure 4.8: Comparison between the results of the change in oscillations amplitude ΔA as a function of the amplitude (A) for the Hook screw based physical pendulum A) in air and C) in water, and the Ball bearing based physical pendulum B) in air and D) in water.

so, f_0 is negligibly small. Furthermore, the absence of any quadratic dependence rules out the presence of any appreciable drag proportional to the square of the velocity.Comparing these results with the results of the ball-bearing-based physical pendulum shown in Figures 4.8 B) and D) it is obvious that the fulcrum friction

force is not negligible in this case since the ratio of the y-intercept to the slope is larger by more than 1000 times than the ratio in the hook-screw-based pendulum.

For our physical pendulum viscometer (with hook-screw-based suspension), the results of three different trials of oscillations data, while immersed in water, were averaged and gave a slope equal to 0.00415 and a y-intercept of 4.2×10^{-5}. Taking into account that we have a combination of two spheres oscillating in the liquid and rod oscillating in the air, then the $\Delta A\ vs. A$ slope (equation 2-18) for our design is

$$Slope\ (S) = \frac{T^2}{4\pi^2}\left(\frac{12\pi r \ell^2 \eta_{Liquid}}{m} + \frac{a_{rod} L_{cm}^2 \eta_{air}}{M}\right) \qquad 4\text{-}2$$

Where T is the period of oscillations, m is the mass of each one of the immersed spheres, M is the total mass of the pendulum, r is the radius of the immersed balls, ℓ is the distance from the fulcrum point to the center of the immersed spheres, L_{cm} is the center of mass position of our pendulum's rod, and a_{rod} is a measure of the size of the pendulum's rod and it has been estimated from the slope of $\Delta A\ vs. A$ slope for air according to equation 4-2, where $\frac{a_{rod} L_{cm}^2 \eta_{air}}{M} = 0.08586$.

So,

$$\eta_{Liquid} = \frac{m}{12\pi r \ell^2}\left(4\pi^2 \times \frac{S}{T^2} - \frac{a_{rod} L_{cm}^2 \eta_{air}}{M}\right) \qquad 4\text{-}3$$

And the error equals

$$\Delta\eta_{Liquid} = \frac{m}{12\pi r\ell^2}\left(\frac{\Delta m}{m} + \frac{\Delta r}{r} + \frac{2\Delta\ell}{\ell}\right)\left(\frac{4\pi^2 S}{T^2}\left(\frac{\Delta S}{S} + \frac{2\Delta T}{T}\right) + \frac{a_{rod}L^2\eta_{air}}{M}\left(\frac{\Delta a_{rod}}{a_{rod}} + \frac{2\Delta L}{L} + \frac{\Delta M}{M}\right)\right) \quad 4\text{-}4$$

But the directly calculated viscosity from the slope contains a large systematic error since it is also linked with other parameters related to the air drag on the pendulum arm that should not be neglected. Because of that, we will use a calibration fit to measure the viscosity via the physical-pendulum-based viscometer in section 4.6.

Figure 4.9 shows the linearity of "$\Delta A\ Vs. A$" curves for the eight different liquids: A) pure etheleyne glycol (E.G. 100%), B) Paraffin oil, and the motor oils SAE C) 10W, D) 0W-20, E) 5W-30, F) 5W-40, G) 15W-40, and F) 10W-60. It is obvious that the unwanted oscillations progressively disappeared as the viscosity of the liquid increased.

Table 4.1: The slope, y-intercept, the calculated viscosity values, and the errors in these values for all liquids.

Liquid	Slope	Error in slope	y-intercept	Error in y-intercept	η_{Liquid} (Pa.s)	$\Delta\eta_{Liquid}$
Water	0.00415	0.00007	4.2×10^{-5}	0.9×10^{-5}	0.0043	0.0006
E.G. 100%	0.01858	0.00008	2.3×10^{-6}	0.6×10^{-6}	0.0955	0.0006
Paraffin	0.02108	0.00007	8×10^{-5}	3×10^{-5}	0.1115	0.0006
10W	0.0455	0.0003	2×10^{-5}	4×10^{-5}	0.2594	0.0006
0W – 20	0.0570	0.0002	1.6×10^{-4}	0.4×10^{-4}	0.3296	0.0006
5W – 30	0.094	0.001	5.3×10^{-4}	1.1×10^{-4}	0.5170	0.0006
5W – 40	0.1123	0.0007	-4×10^{-4}	1×10^{-4}	0.6075	0.0006
15W – 40	0.2125	0.0013	7.4×10^{-5}	1.5×10^{-5}	1.0117	0.0006
10W – 60	0.2247	0.0013	3.6×10^{-4}	0.7×10^{-4}	1.0605	0.0006

Thus, it is obvious that the vibrations that appeared in light liquids (Figures 4.6, 4.9 A), and 4.9 B) completely disappeared in the case of the viscous motor oil SAE 10W-60 (Figure 4.9 H). More importantly, The Reynolds number (Re) seems to still be less than 1 even for the liquids with high viscosity, as deduced from the linear relationship between ΔA *and* A. Table 4.1 lists the values of the slope, y-

intercept values, the errors in these values, and the calculated viscosity (η_{Liquid}), and its error ($\Delta\eta_{Liquid}$)for the curves of all studied fluids. The errors in the slope and y-intercept were calculated using the LINEST function in EXCEL.

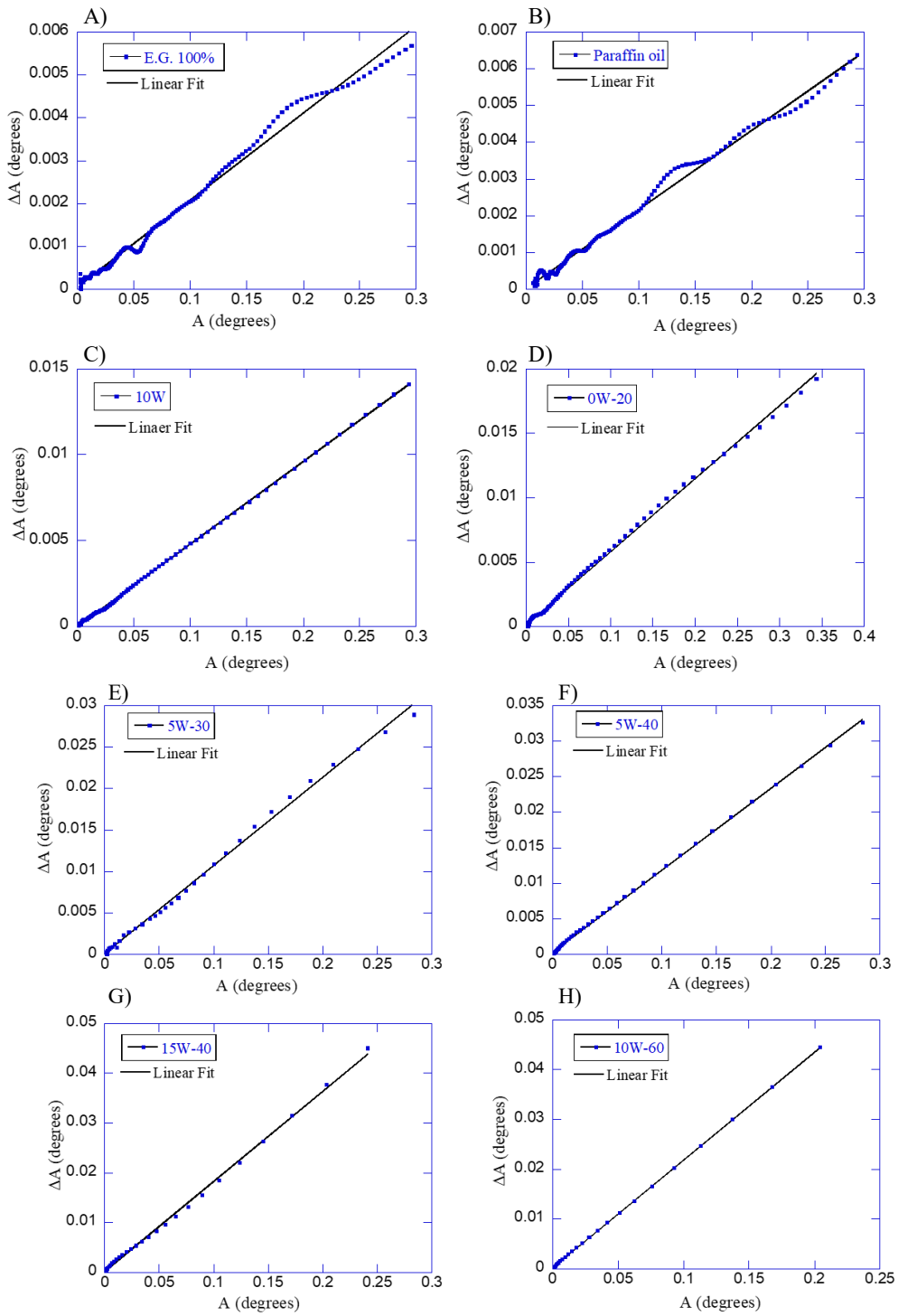

Figure 4.9: The change in oscillations amplitude ΔA as a function of the amplitude of the oscillations A, while the pendulum arms are immersed in A) pure ethylene glycol (E.G. 100%), and different types of light and viscous oils: B) Paraffin oil, C) SAE 10W, D) SAE 0W-20, E) SAE 5W-30, F) SAE 5W-40, G) SAE 15W-40, and H) SAE 10W-60.

4.3 Amplitude decay and damping constant analysis

The energy loss curves studied in section 4.2 were all linear when the physical pendulum arms are immersed in a variety of liquids. This is direct evidence that the oscillations lie in the linear regime (i.e. Reynolds' number "Re" can be considered to be less than 1). This linear relation allows to directly find the viscosity of the liquid from the damping constant (γ_1) (Where $A = A_0 \exp(-\gamma_1 t)$ in this case), since the quadratic velocity-dependent drag term is negligible, thus allowing a simple solution of the equation of motion, as in section 2.2. We have a direct linear relationship between our physical pendulum's oscillations damping constant and the viscosity of the liquid. The damping constant can be written as the sum of three constants: $\gamma_1 = \gamma_A + \gamma_{sphere\{1\}} + \gamma_{sphere\{2\}}$, where γ_A is damping constant caused by the drag on the pendulum arm and $\gamma_{sphere\{1,2\}}$ is the damping constant caused by the drag on the immersed spheres. We ignored here the damping caused by the thin wire connecting each sphere to the pendulum. So,

$$\gamma_1 = \frac{12\pi r\, \ell\, \eta_{Liquid}}{2I_{sphere}} + \frac{(4\pi R + L)\, \eta_{air} L_{cm}}{2I_{rod}} + C_1 \qquad 4\text{-}5$$

Where I_{sphere} is the moment of inertia of the oscillating spheres and equals mL^2, I_{rod} is the moment of inertia of the long hollow cylindrical rod and equals $\frac{1}{3}ML_{CM}^2$, L_{cm} is the center of mass position for the whole pendulum, M its mass, and C_1 is a constant related to the other frictional forces we neglected earlier, especially to the frictional force in the fulcrum, which is quite small.

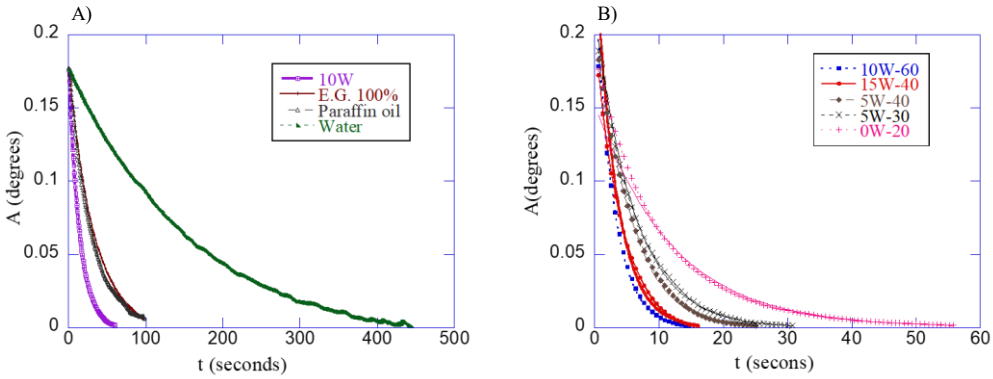

Figure 4.10:The amplitude decay as a function of time for all the studied liquids: A) light liquids, and B) viscous oils.

Figure 4.10 shows the amplitude decay of the pendulum oscillations as a function of time for A) water, E.G. 100%, light oils, and B) viscous oils. The results are separated into two figures for clarity, since the times are very different. It is clear that the decay is exponential and becomes much faster when increasing a liquid's viscosity. This is reasonable since with the rise in viscosity the drag force acting on the small spheres and arms becomes larger, so the damping becomes much faster.

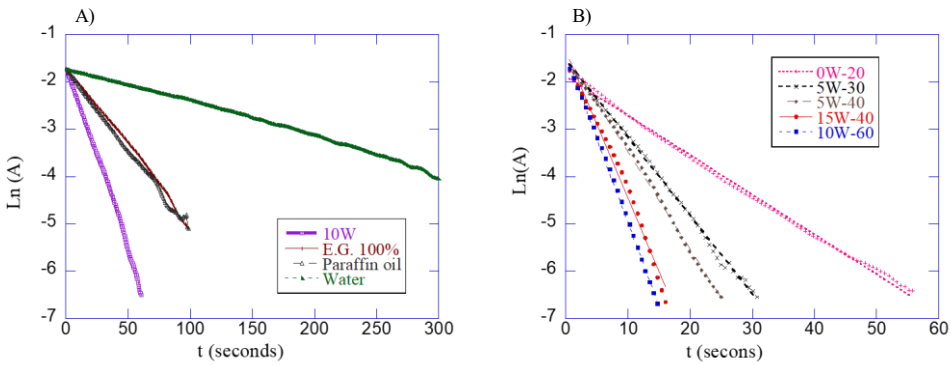

Figure 4.11: The natural logarithm ln(A) as a function of time for A) light liquids and B) viscous oils.

In order to measure the viscosity, a graph of the natural logarithm of the amplitude was plotted as a function of the time (figure 4.11 A) and B). The slope of this relation represents the damping constant ($Ln(A) = Ln(A_0) - \gamma_1 t$). The damping

constants of the oscillations in the different liquids are recorded -with the errors in them- in Table 4.2, where the errors were calculated using the LINEST function in EXCEL.

Table 4.2: The damping constant and its uncertainty for all 9 liquids.

Liquid	Damping Constant (1/s)	Error
Water	0.007363	0.000015
E.G. 100%	0.02989	0.00007
Paraffin Oil	0.0370	0.0002
10W	0.0700	0.0005
0W – 20	0.0907	0.0009
5W – 30	0.174	0.003
5W – 40	0.1861	0.002
15W – 40	0.2849	0.0012
10W – 60	0.314	0.002

4.4 Viscosity effect on the period of oscillations

In addition to the two previous methods used in measuring the viscosity, the change in pendulum oscillations period with the viscosity can also be used to measure it. As discussed before the change in the period was obvious and it agreed with the behavior discussed in chapter 2.

$$T = \frac{A}{\sqrt{B^2 - (C + D\eta)^2}} \qquad 4\text{-}6$$

Where A, B, C, and D are the constants related to the pendulum's center of mass position, the Pendulum's mass, immersed spheres' masses, the immersed spheres' measure of size ($a_{spheres}$), the pendulum arm measure of size (a_{rod}), normal angular frequency, and the immersed arm length as mentioned in the third chapter.

The periods measured for each liquid were listed in Table 4.3. The error in calculating the period is connected with the analysis method and data collection tools. And it can be estimated from the smallest deviation in the analysis tool 'Tracker' to be equal to 0.001 seconds.

Table 4.3: The period of oscillations for our physical pendulum when it is immersed in the different liquids.

Liquid	Period (s)	Calculated Viscosity
Water	1.263	0.00135
E.G. 100%	1.266	0.02086

Paraffin Oil	1.267	0.02700
10W	1.282	0.09972
0W – 20	1.283	0.10375
5W – 30	1.333	0.25374
5W – 40	1.346	0.28380
15W – 40	1.445	0.46429
10W – 60	1.452	0.47499

Figure 4.12 plots the measured periods in the case of water, ethylene glycol, and SAE 10W-60 as a function of their literature viscosity values (Viswanath 2007,

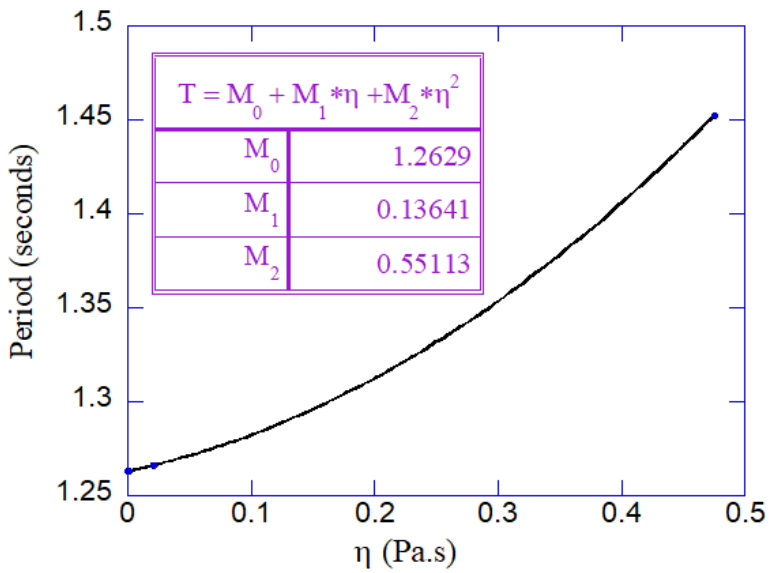

Figure 4.12: Experimentally measured period of oscillations for water, E.G. 100%, and 10W-60 as a function of their literature viscosities.

White 2009, Sawicka, Cieśliński and Smolen 2020, Zahariea and Husaru 2017). This graph shows that one can measure the viscosity from the change in the oscillation period. A polynomial fit of the data points was used to calculate the viscosity of all the studied liquids from the period of oscillation.

4.5 Capillary Viscometer Relative Viscosity

The capillary viscometer relies on measuring the liquid flow rate through a capillary tube, where this flow rate depends on the viscosity (η) and the density (ρ) of the liquid (equation 3-3).

In capillary viscometers we initially find a relative viscosity, which is determined by comparing the liquid flow rate with that of water.

$$\eta_{relative} = \frac{t_{liquid} \times \rho_{liquid}}{t_{water} \times \rho_{water}} \qquad 4\text{-}7$$

In order to measure the viscosity using the capillary, the flow time and the density of all liquids were measured and the capillary relative viscosity was calculated according to equation (4-2). These values are recorded in Table 4.4.

Table 4.4: The flow time, density, capillary relative viscosity and the measured viscosity for all the studied liquids.

Liquid	t (seconds)	ρ (kg/m^3)	$\eta_{relative}$	η (Pa.s)
Water	9.43	998	1	0.00104
E.G. 100%	105.25	1110	12.4	0.02115
Paraffin Oil	243.00	834	21.5	0.03722
10W	534.13	861	48.9	0.08537
0W – 20	918.17	794	77.4	0.13576
5W – 30	1382.16	735	107.9	0.18947

5W – 40	1481.39	804	126.5	0.22226
15W – 40	2772.79	864	254.5	0.44779
10W – 60	2996.34	848	269.9	0.47499

4.6 Calibration, measured viscosity, and performance evaluation

The physical pendulum viscometer must be calibrated and tested with liquids with known viscosities in order to be used reliably and accurately. We used a total of three methods –based on the same pendulum data- to obtain the viscosity from the pendulum oscillations and compare all three with the results from the capillary viscometer and with values from the literature. We start by comparing the slope of $\Delta A\ Vs. A$ with the capillary viscometer results. Our physical pendulum viscometer as -shown in Figure 4.13- gives a perfect linear correlation with the measured

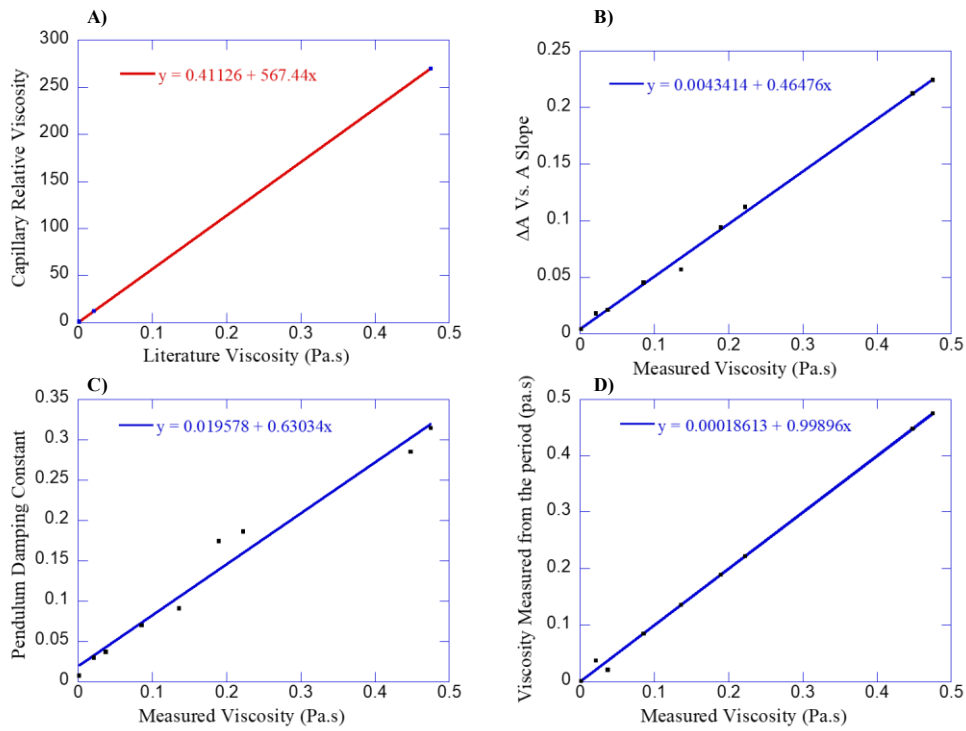

Figure 4.13: A calibration curve to estimate the liquids' viscosity A) calibration between the relative capillary viscosity and the known literature viscosities values and B), C), and D) calibration between ΔA Vs.A curve slope, pendulum damping constant, and the viscosity measured from the period with the measured viscosity using the capillary respectively.

viscosity using the capillary. The linear fit equation can then be used as a calibration to calculate the viscosity of the studied liquids and any other liquid under the same temperature and pressure conditions. One might expect the new viscometer to have two main systematic errors that might affect the accuracy of itsviscosity measurements: The first is the constant drag force on the fulcrum point which was estimated from "$\Delta A\ vs. A$" curves and shown to be negligible -about $9.65 \times 10^{-5}\ intercept$. The second systematic error is the air drag on the pendulum arm which is present in all studies since the main pendulum rod is always in air. This constant related to air drag is estimated to be equal to $(a_{arm}\eta_{air}L_{cm}/2I)$ as mentioned in equation 4-5. This shows that the air drag can pause a problem at low viscosities but not at higher viscosities. However, it is very important to notice that the air drag is common/present in all liquids so, it does not pause any real problem once the device is calibrated.

Table 4.5 records the viscosity of the 9 liquids as measured by: 1) the energy-loss method, 2) the exponential damping fit, 3) the change in oscillation period, and 4) the capillary viscometer. The first three methods used the same data from the pendulum. All Four methods agree with each other and give fairly close results. However, the damping constant and period methods give slightly different values from the energy-loss method and the values measured using the well-known capillary viscometer, indicating that the energy loss-based method gives better results than the other two methods. This can be explained by the constant C_1 in equation 4-5, where it is not only related to the velocity independent frictional force. But it may be also related to the quadratic force (inertial drag force) acting on the pendulum's

rod. In which at the beginnings of the oscillations, the velocity of the pendulum's rod oscillations is large since it is moving at larger angles compared with the ends of the oscillations. This affects the damping of the pendulum and so the damping constant and the period of oscillation. Thus, as recorded in Table 4.5 and clarified in Figure 4.14, the energy-loss-based method of analysis gives the most accurate and precise measurements of viscosity compared to the other two methods. Using this method of analysis, our new physical pendulum viscometer can reliably measure the viscosities in the range of 1 (± 0.15) "mPa.s" to 474 (± 3) "mPa.s". This means that we have developed a high-precision viscometer with the ability to measure the viscosity of a very wide range of viscous liquids.

Table 4.5: The measured viscosities using the capillary viscometer and our physical pendulum viscometer (via three analysis ways) for all the liquids.

Liquid	$\eta_{capillary}$ (Pa.s)	$\eta_{our\ pendulum}$ (Pa.s) measured using the fit		
		From the slope of $\Delta A\ Vs.\ A$	From the damping constant	From the period
Water	0.00104	0.00113	0.00649	0.00135
E.G. 100%	0.02115	0.02877	0.02885	0.02086
Paraffin Oil	0.03722	0.03418	0.04001	0.02700
10W	0.08537	0.08698	0.09178	0.09972

0W – 20	0.13576	0.11184	0.12426	0.10375
5W – 30	0.18947	0.19250	0.25494	0.25374
5W – 40	0.22226	0.23142	0.27392	0.28380
15W – 40	0.44779	0.44808	0.42893	0.46429
10W – 60	0.47499	0.47446	0.47458	0.47499

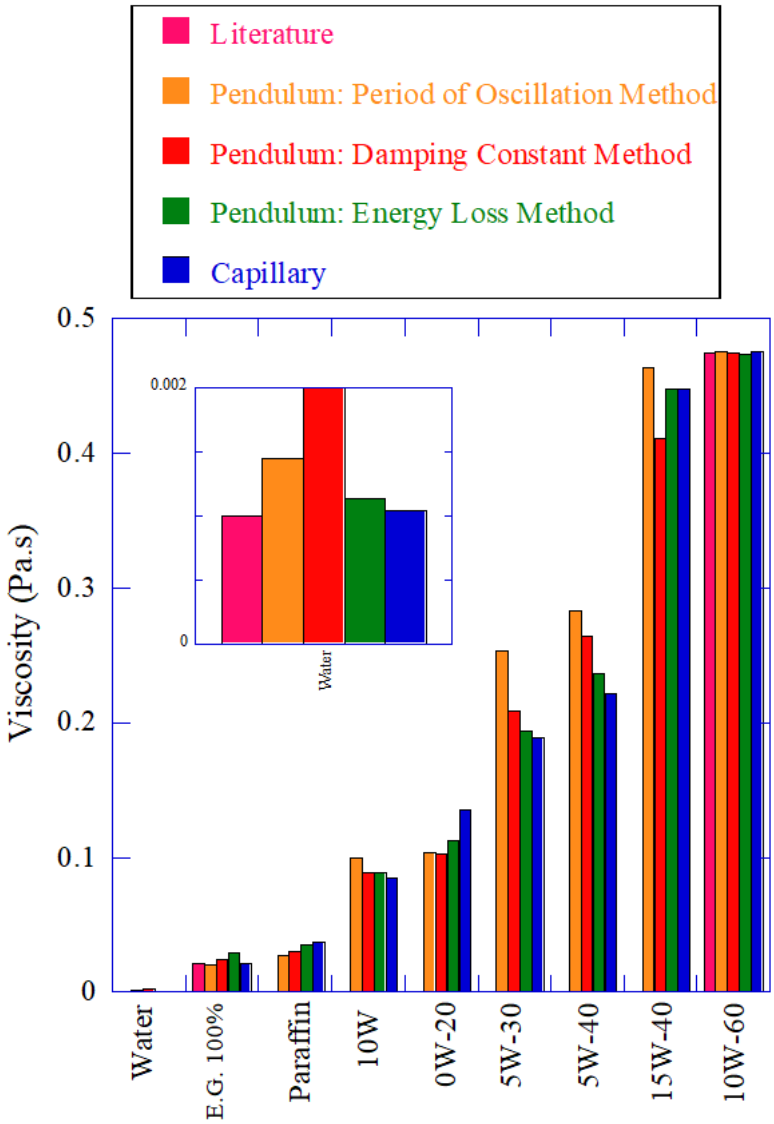

Figure 4.14: A histogram clarifies the differences between the measured viscosities in this thesis, using the capillary viscometer or our physical pendulum viscometer using the different analysis methods

Furthermore, it is important to notice the difference between the directly calculated viscosity from the energy-loss-curve slope recorded in Table 4.1 and that calculated from the calibration fit recorded in Table 4.5. This inaccuracy in the directly calculated values comes from the fact that the constant in equation 2-18 -the constant in equation 4-1 in our pendulum- generally does not directly equal the constant (a) in

the linear fit (y = ax +b), since we have another force acting on the system (velocity independent force).Thus, using a calibration between $\Delta A\ vs.\ A$ slope and the known viscosities, and finding a calibration fit equation is more accurate method to calculate the viscosity of a liquid.

Figure 4.15 shows a comparison between our physical pendulum viscometer viscosities, the capillary viscosities, and the literature viscosities. In general, our new design seems to have accurate and precise results, particularly at higher viscosities it gives perfect results as shown in Figure 4.15D).

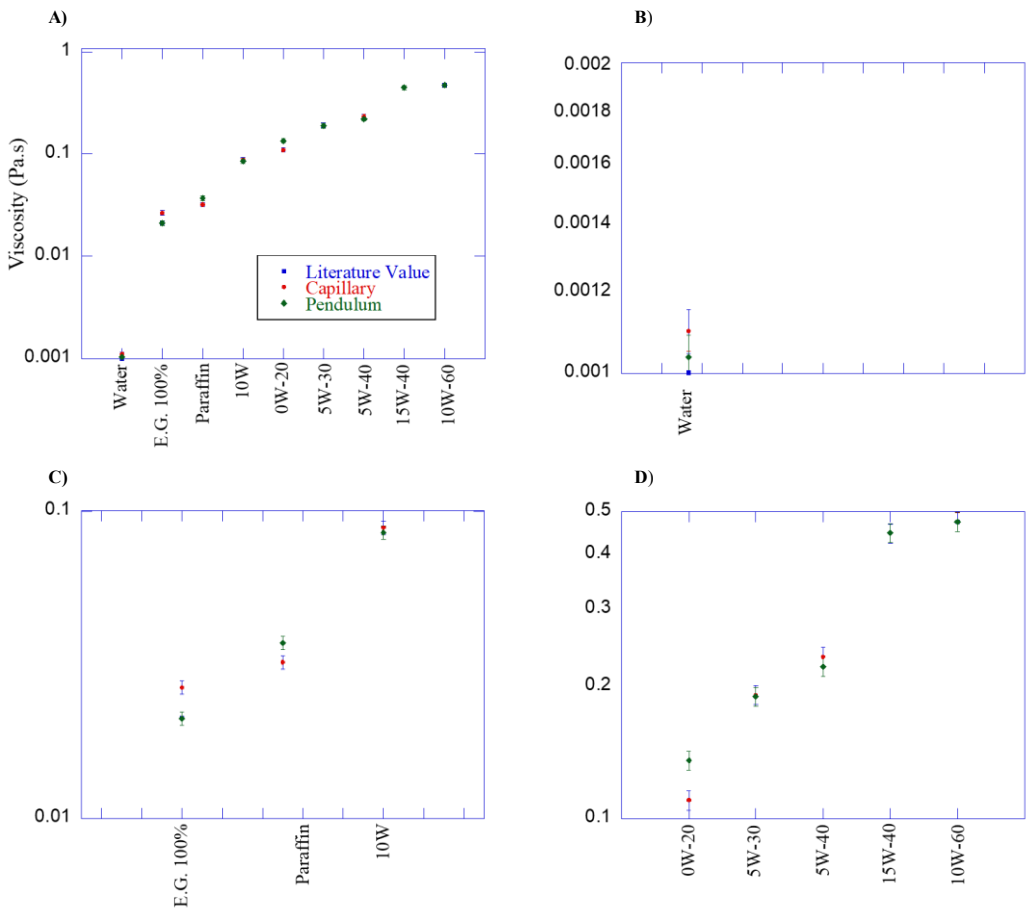

Figure 4.15: A comparison between our physical pendulum viscometer viscosities, the capillary viscosities, and the literature viscosities.

5 Potential Applications

Controlling the damping rate of our physical pendulum viscometer by scaling down the torque caused by the liquids drag force, and by the feature of the ability to control the mass, and length of immersed arms. These features boost our new instrument to be used in many potential applications such study the magneto-viscosity of the magneto Rehlogical (MR) fluids and the ferrofluids, studying the viscosity of some types of the non-Newtonian fluids like the Oobleck, and in some studies in the granular physics. In this chapter, we will discuss the first one, which will be the first future study, using the new instrument, by our research group.

5.1 Magneto-viscosity of MR fluids

Magneto-Rheological (MR) fluids are fluids that are made up of micrometer-scale magnetizable (usually iron) particles in a carrier liquid (Bossis, et al. 2002). These fluids are a kind of smart materials, where some of their properties (like the viscosity) change with an applied magnetic field. Such that the MR fluid can be converted from a Newtonian fluid into a semi-solid or solid material in a fraction of milliseconds under an external magnetic field (Bossis, et al. 2002, De Vicente, Klingenberg and Hidalgo-Alvarez 2011). Under the presence of the magnetic field, the fluids show a Bingham non-Newtonian fluids behavior (De Vicente, Klingenberg and Hidalgo-Alvarez 2011). And it appears a wide range (some orders of magnitude) changes in viscosity with changing the magnetic field strength (Bossis, et al. 2002, De Vicente, Klingenberg and Hidalgo-Alvarez 2011). Because of this property, the MR fluids have many applications such that it used as an active control in the shock

absorbs, seismic vibration dampers, and control valves (De Vicente, Klingenberg and Hidalgo-Alvarez 2011). Also, it was used in some biomedical applications, chemical sensing applications, controlling the thermal transfer, and others (De Vicente, Klingenberg and Hidalgo-Alvarez 2011).

Our newly developed physical pendulum viscometer can be used to study the change in MR fluids viscosity variation with the strength of the applied magnetic field as shown in Figure 5.1. The pendulum arm, thin wires, and balls immersed

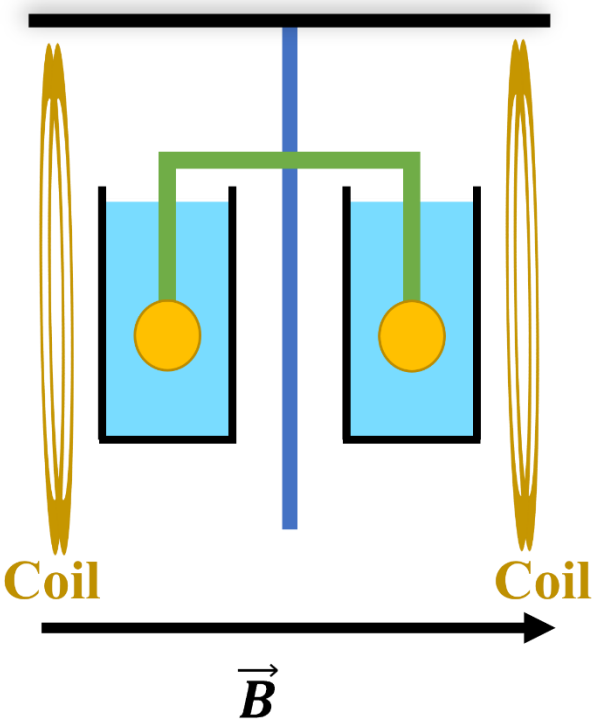

Figure 5.1: Magnetic Field Applied across the fluid's boxes.

were fabricated from non-magnetic materials. As the new viscometer can be used to study the magneto-viscosity of MR fluids without any unwanted effects on the pendulum damping besides its effect on the viscosity of the MR fluid. Furthermore, an additional mass can be suspended from the pendulum to increase its total weight, which increased the range of viscosities and can be studied by minimizing the

fluid's drag force torque on the balls comparable to the torque on the arm and additional mass. And thus, a good number of oscillations to study the MR fluid viscosity at higher magnetic fields.

Conclusions

In this Thesis, A new unique design of the physical pendulum viscometer was developed and fabricated. The main idea of this new design was to scale down the torque caused by the fluids' drag force and minimize the velocity of the immersed particles. Which expanded the range of viscosities that can be studied. Also, using a powerful and comprehensive method of analysis depends on the energy loss by each pendulum oscillation to analyze the pendulum's damping mechanism, whereas the limitation in the highly laminar regime was removed. This new physical pendulum viscometer appeared to be an accurate and precise instrument to be used to measure the viscosity in the industrial fields, scientifical research, and the physics laboratories.

This new viscometer will be used to study the viscosity of the magnetorheological fluids and ferrofluids as a function of the magnetic field strength and orientation. The work on this new study was started, in the physics department research laboratories at Birzeit University, by our research group as a new project.

References

Andrade, H. A. , and S. Kovner. 1998. “Software synthesis from dataflow models for G and LabVIEW/sup TM/.” *Conference Record of Thirty-Second Asilomar Conference on Signals, Systems and Computers (Cat. No.98CH36284).* Pacific Grove, CA, USA: IEEE.

Bista, Archana, Noel McCarthy, Colm P. O'Donnell, and Norah O'Shea. 2021. “Key parameters and strategies to control milk concentrate viscosity in milk powder manufacture.” *International Dairy Journal* 121.

Bos, R. W., and P. R. Wellens. 2021. “Fluid–structure interaction between a pendulum and monochromatic waves.” *Journal of Fluids and Structures* 100 (103): 191.

Brown, Douglas. 2008. “Video modeling: combining dynamic model simulations with traditional video analysis.” *In American Association of Physics Teachers (AAPT) Summer Meeting.*

Brown, Douglas, and Anne J. Cox. 2009. “Innovative Uses of Video Analysis.” *The Physics Teacher* 47 (3): 145-150.

Crawford, Frank S. 1975. “Damping of a simple pendulum.” *American Journal of Physics* 43 (3): 276-277.

Hameed, D. 2021. “Engine Oil Deterioration based on the Viscosity, flash point and fire point for Different Trip Length.” *Kurdistan Journal of Applied Research* 6 (1): 13-20.

Hasnain, Saqib, Karam Dad Kallu, Muhammad Haq Nawaz, Naseem Abbas, and Catalin Iulin Pruncu. 2020. “Dynamic Response of an Inverted Pendulum System in Water under Parametric Excitations for Energy Harvesting: A Conceptual Approach.” *Energies* 13 (19): 5215.

Hong, Xinguo, and Kunquan Lu. 1995. “Viscosity Measurement With Double wire Torsion Pendulum.” *Review of Scientific Instruments* 66: 4318.

Hou, Zhe, Kai Yuan, Fuyong Xie, Hai Jin, and Qingfan Shi. 2015. “Oscillation properties of a simple pendulum in a viscous liquid.” *European Journal of Physics* 36 (1): 015011.

Irgens, Fridtjov. 2014. “Classification of Fluids.” In *Rheology and Non-Newtonian Fluids*, 1-16. Cham: Springer International Publishing.

Janik, Joanna, Agnieszka Krol-Otwinowska, Dagmara Sokolowska, and Jozef K. Moscicki. 2006. “Pendulum viscometer: A new method for measurement of Mięsowicz nematic shear viscosity coefficients η1 and η2.” *Review of Scientific Instruments* 77 (12): 123906.

Johnson, Gary W. , and Richard Jennings. 2006. *LabVIEW Graphical Programming.* 4th. Newyork: McGraw-Hill.

Leme, José Costa, and Agostinho Oliveira. 2017. “Pendulum Underwater – An Approach for Quantifying Viscosity.” *The Physics Teacher* 55 (9): 555-557.

Martins, D. A. M., A. M. Silveira-Neto, and V. Steffen Jr. 2007. “A Pendulum-Based Model for Fluid Structure Interaction Analysis.” *Revista de Engenharia Térmica* 6 (2): 76.

Miller, B. J. 1974. “More Realistic Treatment of the Simple Pendulum without Difficult Mathematics.” *American Journal of Physics* 42: 298-303.

Muriel, Diego F., and Joseph Katz. 2021. “Time Evolution and Effect of Dispersant on the Morphology and Viscosity of Water-In-Crude-Oil Emulsions.” *Langmuir* 37 (5): 1725-1742.

NIManuls. 2018. *LabVIEW help.* NI Publications.

Pain, H. J. 2005. *The Physics of Vibrations and Waves.* 6th. Chichester: John Wiley & Sons Ltd.

Ramli, Hanif, Kar Tim Chan, and Wing Fen Yap. 2016. “Study of simple pendulum using tracker video analysis and high speed camera: an interactive approach to analyze oscillatory motion.” *Solid State Science and Technology* 24 (2): 297-305.

Reynolds, Osborne. 1883. “An Experimental Investigation of the Circumstances Which Determine Whether the Motion of Water Shall be Direct or Sinuous, and of Resistance in Parallel Channels.” *Philosophical Transactions of the Royal Society of London* 174: 935 -983.

Royer, John R., Eric I. Corwin, Peter J. Eng, and Heinrich M. Jaeger. 2007. “Gas-Mediated Impact Dynamics in Fine-Grained Granular Materials.” *Physical Review Letters* 99 (3).

Rudyak, V. Ya., A. V. Minakov, A. A. Gavrilov, and A. A. Dekterev. 2008. “Application of new numerical algorithm for solving the Navier—Stokes equations for modelling the work of a viscometer of the physical pendulum type.” *Thermophysics and Aeromechanics* 15 (2): 333-345.

Sawicka, Dorota, Janusz T. Cieśliński, and Slawomir Smolen. 2020. “A Comparison of Empirical Correlations of Viscosity and Thermal Conductivity of Water-Ethylene Glycol-Al2O3 Nanofluids.” *Nanomaterials (Basel, Switzerland)* 10 (8): E1487.

Serway, Raymond A., and John W. Jewett, Jr. 2014. *Physics for Scientists and Engineers With Modern Physics.* 9th . New York: CENGAGE Learning.

Sharma, Prateek, Tzvetelin T. Dessev, Peter A. Munro, Peter G. Wiles, Graeme Gillies, Matt Golding, Bryony James, and Patrick Janssen. 2015. “Measurement techniques for steady shear viscosity of Mozzarella-type cheeses at high shear rates and high temperature.” *International Dairy Journal* 47: 102-108.

Sommerfeld, A. 1908. “A Contribution to the Hydrodynamic Explanation of Turbulent Fluid Movement.” 9.

Squire, Patrick T. 1986. “Pendulum damping.” *American Journal of Physics* 54 (11): 984-991.

Stokes, G. G. 1851. “On the Effect of the Internal Friction of Fluids on the Motion of Pendulums.” *Transaction of the Cambridge Philosophical Society* 9 (2): 8-106.

Travis, Jeffrey , and Jim Kring. 2007. *LabVIEW for everyone : graphical programming made easy and fun.* 3rd. New Jersey: Prentice Hall.

Viswanath, D. S. 2007. *Viscosity of liquids: theory, estimation, experiment, and data.* Dordrecht: Springer.

White, Frank M. 2009. *Fluid Mechanics.* New York: McGraw-Hill.

Yh, Eng, and Ws Lau. 2008. “Estimation of the Hydrodynamics Coefficients of an ROV using Free Decay Pendulum Motion.” *Engineering Letters* 7.

Zahariea, Dănuț, and Dorin Emil Husaru. 2017. “Temperature-dependent viscosity analysis of SAE 10W-60 engine oil with RheolabQC rotational rheometer.” *MATEC Web of Conferences* 112: 10014.

Ziaee, Mohsen, and Nathan B. Crane. 2019. “Binder jetting: A review of process, materials, and methods.” *Additive Manufacturing* 28: 781-801.

Zonetti, L F C, A S Camargo, J Sartori, D F de Sousa, and L A O Nunes. 1999. “A demonstration of dry and viscous damping of an oscillating pendulum.” *European Journal of Physics* 20 (2): 85-88.

Additional Chapter: Introducing an Experiment on The Thermoelectric Effect to The Physics Advanced Labs

In this additional chapter we present a new experiment that we developed and published in the 'European Journal of Physics'. This experiment has been developed for the advanced or sophomore physics laboratories. In this experiment the student can study the Thermoelectric effects: Peltier and Seebeck effects, and some other scientific investigations: Supercooling and flash freezing of water, and the temperature dependence of the resistivity of metals and semiconductors.

Thermoelectric effects and applications: an advanced physics laboratory experiment

R Aqra[1], K AbualRob[1], H Jaeger[2] and KF Eid[1,2,*]

[1] Department of Physics, Birzeit University, Birzeit, Palestine

[2] Department of Physics, Miami University, Oxford, OH 45056, United States of America

E-mail: keid@staff.birzeit.edu

Received 26 October 2021, revised 4 February 2022

Accepted for publication 24 May 2022

Published XX XX XXXX

Abstract

We developed a simple, inexpensive undergraduate laboratory experiment covering concepts and applications related to thermoelectric effects. Students usecommercially available thermoelectric plates for producing electric current orfor cooling and heating, then utilize them to perform experimental investigations that involve cooling. These investigations include studying supercoolingand flash-freezing of water, as well as the temperature dependence of the resistivity of metals and semiconductors. The experiment allows students to easilyadd more components to investigate additional phenomena, thus lending itselfas a potential open-ended 'final project' in the lab. The activities emphasize experiment design and scientific investigation. They also develop some of themain goals of advanced physics laboratories, such as the exposure to new technologies and experimental skills, data collection and automation/control, as well as data analysis and the clear communication of the results. This experiment can be integrated into the physics curriculum of electronics or advanced laboratory courses at the sophomore or higher levels.

Keywords: advanced laboratory physics, physics education, thermoelectric effect, Peltier cooling, Seebeck effect

(Some figures may appear in colour only in the online journal)

*Author to whom any correspondence should be addressed.

0143-0807/22/000000+14$33.00

1. INTRODUCTION

Advanced labs serve an important role in the physics curriculum. They allow students to start learning and practicing scientific investigations and the design of experiments, as well as prepare them to join the skilled workforce [1,2]. More specifically, students develop experimental skills and expertise, learn to design apparatus, generate and acquire data, analyze data properly [3], and communicate their findings in a succinct and clear way through lab reports and oral presentations [4,5]. These skills are acquired through direct hands-on practice in advanced labs, where the students conduct the experiments with instructors' guidance.

The thermoelectric Seebeck and Peltier effects were discovered about two centuries ago, where the flow of electric current across a junction of dissimilar conductors (or semiconductors) can create a temperature gradient across the junction, and vice versa [6]**.** Yet, these effects still have many modern applications ranging from scientific devices [7], to cooling electronic/computer parts, and simpler consumer products, like camping coolers, among numerous others [8]. Furthermore, the field continues to evolve [9] and attract research, like the spin-dependent Seebeck effect [10,11].

The experiment described here has the general theme of studying and using the thermoelectric effect. It can be divided into two main parts: a) Studying/understanding the behavior of the thermoelectric devices and b) using thermoelectric cooling and heating in other investigations. Both parts will be introduced here, preceded by a brief description of the lab settings.

1.1 Lab Settings

This experiment was integrated either into the sophomore electronic instrumentation laboratory at Miami University or in the senior advanced physics lab at Birzeit University. The sophomore electronic instrumentation lab especially teaches the students experimental skills and knowledge that helps them in their future research or careers that involve technology [12]. Miami's 'Electronic Instrumentation

Laboratory' is designed to give extensive exposure to basic electronic devices, tools, and concepts. These include the use of operational amplifiers and semiconductor devices for different purposes, the use of software to run equipment as well as acquire and analyze data, low-resistance measurements and noise reduction, and the use of modern microcontrollers. Thus, the 'thermoelectric effects' experiment served to build upon and enhance some of the skills that the students learned throughout the semester and allowed them to gain insight into some fundamental science through these experiments. In the advanced physics lab, students were expected to contribute more in the design of the experiments and to propose/conduct extra activities and deeper analysis. This experiment is easily integrated in both types of lab courses.

1.2 Thermoelectric Effects

There is a host of effects associated with the flow of energy (heat) and electric charge through materials. The best-known effect of current flow in materials is Joule heating effect, where a current (I) flowing through an 'ohmic' conductor (i.e. a conductor with a linear relation between current and voltage). The current will add energy to the conductor thus heating it according to $P = I^2R$, where R is the resistance of the conductor and P the power dissipation [12].

Yet there are multiple lesser known effects that are related to the flow of charge and energy in materials, such as the Seebeck [14], the Peltier [15], and the Thomson [16,17] effects. Furthermore, these effects are also influenced by magnetic fields and give rise to new thermomagnetic effects as well. Such thermomagnetic effects are somewhat similar to the Hall and the Spin Hall effects and are still the subject of intense research [18]. We will focus here on the Peltier and the Seebeck effects only as they are quite useful in cooling, heating, and other temperature control applications.

1.2.1 The Seebeck Effect

When two conductors are connected together to form two junctions (known as a thermocouple), a potential difference will develop across points A and B, if the

junctions are maintained at different temperatures (Fig. 1). This effect is the thermoelectric effect or the Seebeck effect, named after the scientist who first observed it in the early 19th century [6,9]. If a 'load' is connected between points A and B a current flows through the circuit. So, the Seebeck effect concerns the conversion of thermal energy into electric energy, where a temperature gradient creates an electromotive-force, or a voltage. This effect has many applications in temperature measurement and in small scale power generation.

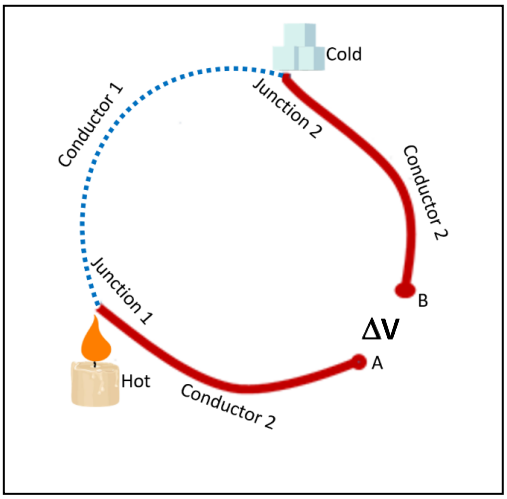

Fig. 1. Thermoelectric or Seebeck effect. A temperature gradient between junction 1 and junction 2, which connect two different conductors, creates a potential difference ΔV between points A and B.

1.2.2 The Peltier Effect

The Peltier effect is practically the reverse of the Seebeck Effect: When a current flows through a thermocouple junction (i.e. a voltage applied across the junction) a temperature gradient develops across the junction [8,18]. In a way, the Peltier effect is basically a heat pump that extracts heat from one side of the junction and 'deposits' that heat on the other side causing one side to cool down and the other side to heat and so making this effect useful in cooling and heating applications. Yet, in practice it is mainly used for cooling because there are other, more efficient ways for heating applications. Some of the common cooling applications of the Peltier

effect are cooling electronic equipment and refrigeration (such as in a portable cooler, for example) [20].

It is important to notice that both the Peltier and Seebeck effects are reversible, which means that if you reverse the current flow direction then the cold and hot ends of the thermocouple will switch. This is unlike the Joule heating effect, where thermal energy is generated whether you run current in one direction or the other through a conductor.

1.2.3 Other Thermoelectric Effects

Another thermoelectric effect is the Thomson effect [17]. It is directly related to the Seebeck and the Peltier effects, except that it refers to the cooling and heating effects when an electric current flows in a conductor that has a temperature gradient across its ends. In particular, the Thomson effect occurs in a *single* conductor, without a need for a thermocouple and leads either to cooling or heating, depending on the relative directions of current flow and temperature gradient. Both Peltier and Seebeck effects depend on external magnetic fields, which leads to two additional thermoelectric (or thermomagnetic) effects. Even though the Seebeck effect was demonstrated about two centuries ago, the associated thermomagnetic effects are quite contemporary and are being heavily studied across the world [21]. They are somewhat similar to the Hall effect and the Spin Hall effect [22].

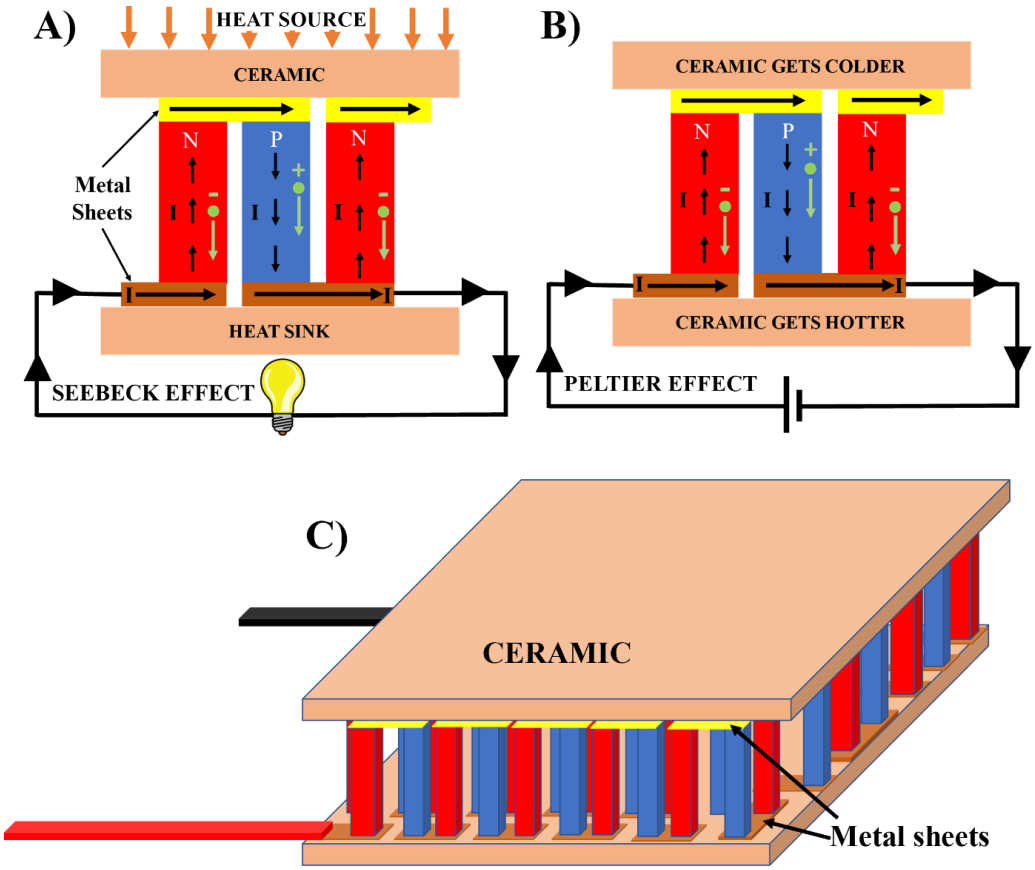

Fig.2: Schematic representation of thermoelectric devices that use p- and n-type semiconductors, which are significantly better than metal or alloy-based devices, both to produce power and for cooling. A) A thermoelectric device of one junction is used for producing electrical power (Seebeck effect). B) A thermoelectric device of one junction is used for cooling (Peltier effect). C) A thermoelectric cooling (TEC) device of many junctions [19, 20, 23].

1.2.4 Materials and Designs for Peltier-effect-based Cooling and Heating

Simple thermocouples are made of two dissimilar metals connected together, such as copper and constantan, a copper-nickel alloy. These thermocouples generate relatively small voltages of a few to a few tens of micro-volts per kelvin (K) of temperature difference between the ends. Semiconductor materials are especially important in Peltier and Seebeck effects applications because they have much larger 'Seebeck coefficients' that lead to stronger thermoelectric effects (Fig. 2) [23,24]. Parts A and B of Fig. 2 show how semiconductor-based Peltier cooling works. It is

important to notice that the free charge carriers move against the current direction in the n-type elements and with the current direction in the p-type elements. Thus the free charge carriers always move in the same direction (e.g. from the top to the bottom of each element in the figures), which is crucial in the Peltier and Seebeck effects [19, 20, 23].

The cooling and power generation effects associated with a single junction are still too small for applications, even when using semiconductors. Instead, a large array of these junctions is usually used in order to produce an appreciable cooling effect in commercial Peltier coolers (Fig. 2C). All junctions are connected thermally in parallel, where, for example, the top part will be cold for all elements and the bottom part will be hot for all of them, or vice versa. Electrically, the junctions are connected in series, so the same current flows through all of them. This is important in order to maximize the cooling because the Peltier effect is proportional to the actual current flowing into a thermocouple.

1.3 Using Thermoelectric Coolers in Other Investigations

TECs were used in three simple studies that required a change in temperature. These studies included the behavior of water droplets when cooled below their freezing temperature as well as the resistance variation with temperature in both a metal and a semiconductor.

1.3.1 Supercooling and flash-freezing of water droplets cooled below their freezing temperature

Water is said to be supercooled/undercooled when it remains liquid below its ice melting temperature of 0°C. This phenomenon was first demonstrated by Gabriel Fahrenheit in the early 18th century [25,26]. He also observed a rapid increase of the water temperature when it finally freezes. This rapid freezing process is called flash freezing, and the temperature rises to the equilibrium melting point when flash freezing occurs. The occurrence of flash freezing depends on the initial nucleation of ice and some special conditions [23]. Flash freezing of a small water droplet on

a cooled surface depends on the heterogeneous nucleation of ice on its surface, as well as on the droplet volume and the contact angle with the cooled surface [27–29].

1.3.2 Resistance R(T) in Metals and Semiconductors

The variation of a material's resistivity with its temperature depends mainly on the energy band structure of that material. The conduction band in metals is partially filled with electrons. These free electrons are the vehicle for conducting electricity, so metals are excellent conductors. On the other hand, insulators have their valence bands full and their conduction bands empty with a large energy gap separating the two bands, thus having no free electrons to conduct electricity and heat. Semiconductors are just like insulators, but with a relatively small energy gap that is not much larger than the thermal energy ($\frac{3}{2}$ $k_B T$) of an electron.

The resistivity of a metal increases linearly with its temperature due to the increase in lattice vibrations that cause a decrease in the mean free path of free electrons [30]. In the case of intrinsic semiconductors: there are no free electrons to carry the current at low temperature, since the conduction band is empty. The increase in temperature thermally excites electrons to the conduction band, which also creates holes in the valence band. These free electrons and holes can carry the current and cause the resistivity to decrease. This decrease in resistivity follows an exponential curve resembling the Boltzmann factor that has half of the energy gap (E_g) divided by Boltzman constant (k_B) [30] in its exponent.

2 EXPERIMENTAL SETUP AND MEASUREMENTS

We used a TEC1-12706 thermoelectric cooler (TEC) –purchased through Amazon- that has 127 pairs of p- and n-type pins and a surface area of its flat face of 40mm x 40mm. The TEC was placed on an aluminum block that is immersed in water as a heat sink. The TEC was biased using a DC power supply. A 'type K' thermocouple was placed on the TEC surface and connected to a National Instruments

'MyDAQ' data acquisition unit to collect the temperature readings using LabVIEW software. Applying the DC bias over the TEC in one direction decreases the temperature of the top side (compared to the heat sink) while reversing the bias polarity increases the temperature [e.g. in Fig. 2B) running the current clockwise causes the top side to get colder than the bottom, while running a counter clockwise current makes the top side of the TEC device hotter than the bottom].

Temperature measurements were made for four different configurations:

1- Temperatures at set TEC currents: Nothing was placed on the surface (except the thermocouple), and the temperature was monitored with the current through the cooler.
2- Temperature gradients to generate electricity: The TEC was placed between two thermally isolated 'reservoirs', where a hole in Styrofoam was used to keep hot water on one side and ice-and-water on the other. Each of these sides was in direct thermal contact with the TEC fixed in the Styrofoam hole (see Fig. 5A) below). The generated thermoelectric voltage and current were studied as functions of the temperature difference.
3- A water droplet was placed on the TEC surface and its temperature was monitored while cooling, using a small thermocouple immersed in the droplet.
4- A thin metal wire and a semiconductor (thermistor) were placed on the surface and their resistances were monitored as the temperature was changed:
    a) Resistance of a metal wire placed on the surface. About 1 meter of thin copper wire (gauge 32, diameter 0.2 mm) was made into a coil, put in thermal contact with the TEC top surface, and connected in series to a 470-Ω resistor and connected to a 5V power supply in a voltage divider configuration [31] (Fig. 3 A). An inverting amplifier made with a type 741 operational amplifier with a gain (G) of about –15 was used to determine the voltage drop at the copper wire, $V_{cu} = \frac{V_{out}}{G}$. After that, we monitor the change in the voltage with temperature while varying the

TEC current gradually for the two cases (heating and cooling) via a LabVIEW program (Fig. 3 B). The resistance of the copper wire is then calculated using:

$$R_{cu}(\Omega) = \frac{V_{cu} \times 470\,\Omega}{(5V - V_{cu})}$$

b) Resistance of a semiconductor. A TTC 502 thermistor was placed on the surface and connected in series to a 100-kΩ resistor and a 5 V power supply in a voltage divider configuration. The change in the semiconductor voltage with the temperature gave the resistance of the semiconductor sample as:

$$R_{SC}(\Omega) = \frac{V_{out} \times 100k\Omega}{(5V - V_{out})}$$

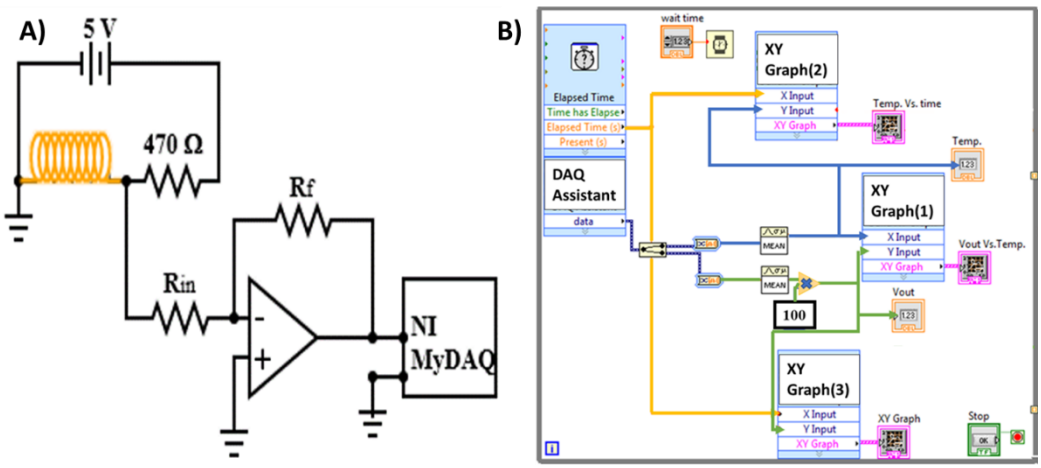

Fig.3: Circuit and software tools used in measurements. A) A Simple electrical circuit for measuring the resistance of the copper wire. B) A basic LabVIEW program to monitor and record the data. This program saves the data and gives three data graphs: 1) XY Graph (1): monitors the output voltage variation as a function of temperature. 2) XY Graph (2): monitors the temperature variation. 3) XY Graph (3): monitors the voltage variation as a function of time.

For those who do not want to use a computerized data acquisition setup, the resistance of the thermistor can be measured with a multi-meter and recorded

manually without the need for computerized data recording. In this case, the multi-meter needs to be connected in the place of the 'NI MyDAQ' unit shown in Fig. 3a). It should be noted here that a multi-meter will also have to be used to measure the potential difference across the thermocouple in order to measure the temperature manually. A manufacturer-provided calibration curve can then be used to find the matching temperature.

3. RESULTS AND ANALYSIS

3.1 Temperature at set TEC currents (Newton's Law of cooling and heating)

Figure 4 shows the variation of the temperature when changing the current: The temperature approaches its new equilibrium value asymptotically, both when cooling and heating. This is in agreement with Newton's law of cooling and heating, which states that the rate of change of temperature is proportional to the temperature difference between the object, T, and its surroundings, T_s. So, if T_F and T_0 are the final and initial temperatures, respectively [32,33]:

$$\frac{dT}{dt} \propto (T - T_s)$$

$$T = T_F + (T_0 - T_F)e^{-kt}$$

This results in an exponential and asymptotic approach of the temperature to the new value dictated by the TEC settings and the surroundings. The Figure shows the behavior for both heating and cooling. Starting from zero current, the temperature of the surface was 25℃. The current was then increased from zero to 1.0 A in steps of 0.5 A. The asymptotic approach to the final temperature is clear in each of these two steps. The current is then dropped from 1.0 A down to 0 A and the same asymptotic behavior is observed.

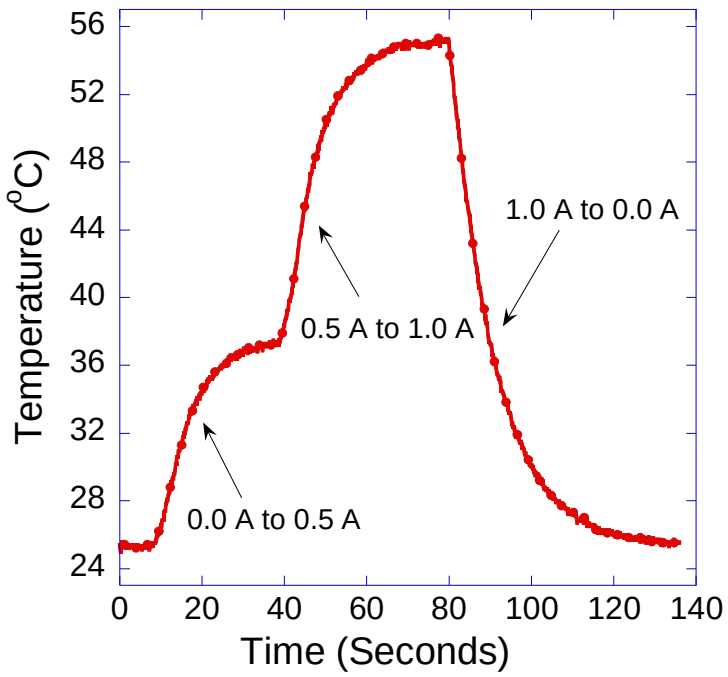

Fig. 4: T(t) variation when the thermocouple is placed on the thermoelectric plate while it is heated or cooled gradually by changing the applied current.

3.2 Thermoelectric Power Generation via a TEC

The second set of activities in lab exercise involves the study of electric power generation by imposing a temperature difference between the bottom and the top of the thermoelectric plate. In fact, the thermoelectric cooler can be used as a thermoelectric generator for a limited temperature difference range. This range is limited by the ceramic plate materials and properties, solder joints, thermoelectric legs *dimensions, and the wires used on the device.* Nesarajah and Frey *[34]* showed in detail the differences between thermoelectric cooling and thermoelectric power generation. *In*

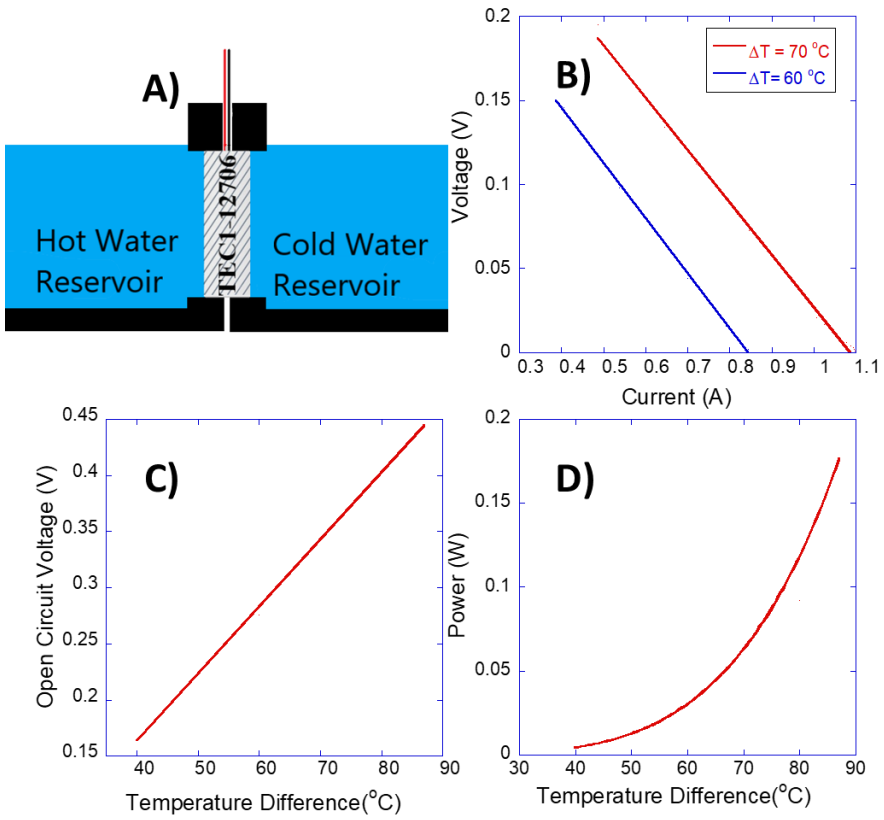

Fig. 5: A) Experimental set-up to measure the open-circuit voltage and the dissipated power from the thermoelectric cooler TEC1-12706, where the TEC was directly in thermal contact with the water (hot and cold) from both sides. B) The I-V characteristics for the TEC at temperature differences of 60°C (lower line) and 70℃ (upper line). C) The open-circuit voltage vs. the temperature difference. D) The dissipated electrical power vs. the temperature difference.

our experiment, the thermoelectric cooler was directly in thermal contact with hot water from the right and cold water with ice on the left, as shown in figure 5 A). The temperature of each side was measured using liquid thermometers. The TEC was connected to a resistor of 2 ohms and a resistance decade box in a voltage divider configuration. The induced voltage and current from the TEC device were measured by measuring the voltage difference across the 2 Ω resistor using the DAQ unit. Figure 5 B) shows the current-voltage (I-V) characteristics of the TEC for two temperature differences. It shows a linear behavior with a slope of about –

0.31 V/A. From the equation of the straight line, the maximum power achieved is about 50 mW (by maximizing the $P = I \times V$ equation) at a current of about 0.5 A. Figure 5 C) shows a plot of the induced open circuit voltage vs. the temperature difference. The thermoelectric cooler in this setup can be used to produce a voltage of 0.45 V at a temperature difference of about 85℃. Finally, Fig. 5 D) shows a plot of the TEC's dissipated electrical power as a function of the temperature difference. It shows that the TEC dissipates approximately 200 mW of power at a temperature difference of about 85℃. The behavior in both figures 5 C) and 5 D) is consistent with the TEC1-12706 Peltier model datasheet [35] and some previous work on it [34]. Furthermore, we note that no hysteresis occurs in either of them. So, these TEC devices can be used as thermoelectric generators in some applications when a sufficiently large temperature gradient is maintained across their sides.

4. FURTHER RESULTS AND ANALYSIS

4.1 Water droplets: Supercooling, flash freezing, and melting

The shape and behavior of water droplets on surfaces have attracted significant research attention and have many applications [36,37]. The supercooling and flash-freezing of water are also fascinating phenomena that are worth studying and understanding. Figure 6 shows two pictures of a 40-µL water droplet taken before (left) and after freezing (right). The thin thermocouple is seen inserted in the droplet from the left. To get a clearer idea about what happens when the droplet freezes, Fig. 7 shows the temperature behavior as recorded by the thermocouple in a water droplet placed on the TEC plate while cooling (red circles). The figure also shows the temperature varia-

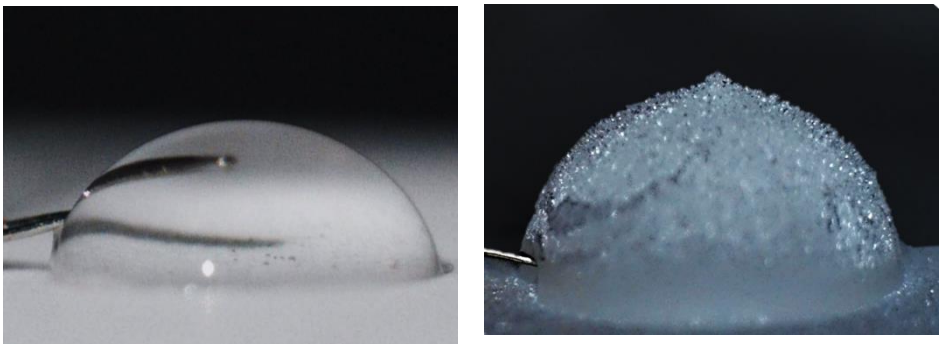

Fig. 6: A picture of the water droplet during the cooling of the thermoelectric plate. (Left) Before the beginning of the freezing process. (Right) After the flash-freezing process.

tion as recorded by the thermocouple when there is no water droplet on the TEC plate (blue). Water is relatively insulating, so the thermocouple is likely to be measuring the temperature of the water in its direct vicinity within the water droplet.

There are two striking observations in the figure: 1) The temperature of the water droplets falls smoothly to well below 0℃, while it is still in the liquid phase-as observed visually and through a digital camera. This is known as supercooling. 2) There is a significant difference between the cooling curves with a water droplet on the surface and without it. Specifically, the curve for the water droplet displays two flat regions at T= 0℃, one immediately after flash-freezing and the second while warming to room temperature after turning off the cooling current. As the temperature reaches about -11℃ it suddenly rises to 0℃. This sudden jump in temperature occurs when a fraction of the water droplet freezes instantly. This is the well-known flash freezing of supercooled water, after which the rest of the droplet freezes relatively slowly. After the flash-freezing temperature jump, the temperature stays at zero for a bit, while the entire droplet freezes and then the temperature of the ice eventually starts dropping again to the expected equilibrium

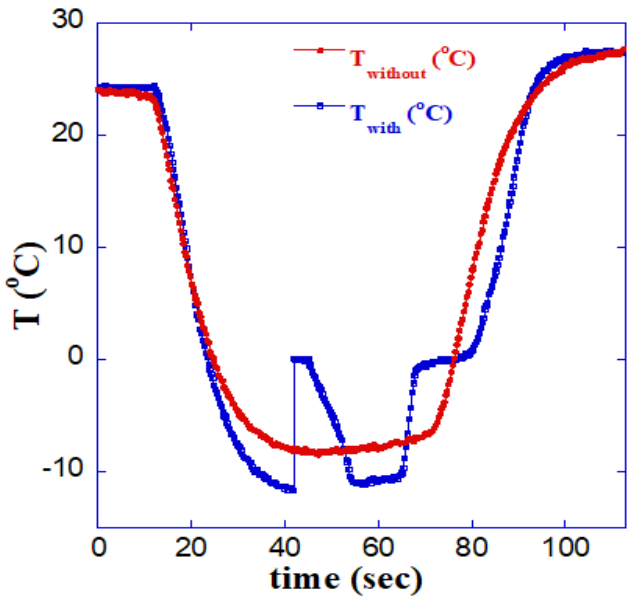

Fig. 7: (Red circles) Temperature variation when the thermocouple is placed on the thermoelectric plate (without a water droplet) while it cooled. (Blue squares) Temperature variation when the thermocouple is placed inside a water droplet during cooling.

value for the particular TEC settings (nearly –17℃). The temperature was allowed to stabilize at this value for about half a minute, then the cooling current was turned off, and the temperature of the ice droplet started to rise immediately. Yet, the temperature curve flattens out again at 0℃ and stays there until the vicinity of the thermocouple melts. At this point the temperature starts to climb again toward room temperature.

4.2 Resistance change with temperature in a metal and a semiconductor

Figure 8 shows the resistance of a copper wire as a function of temperature. The resistance of the wire is quite low and increases linearly with temperature. According to the resistance variation for metals $R = R_0 (1 + \alpha (T - T_0))$, plotting the relative resistance as a function of temperature results in a straight line with slope

equal to αR_0 with α the temperature coefficient of resistivity. The best fit in Fig. 8 gives the value for $\alpha = (3.95 \pm 0.02) \times 10^{-3}$ °C^{-1}, which agrees well with the literature value of 3.93×10^{-3} °C^{-1} for copper at 20°C [5, 37].

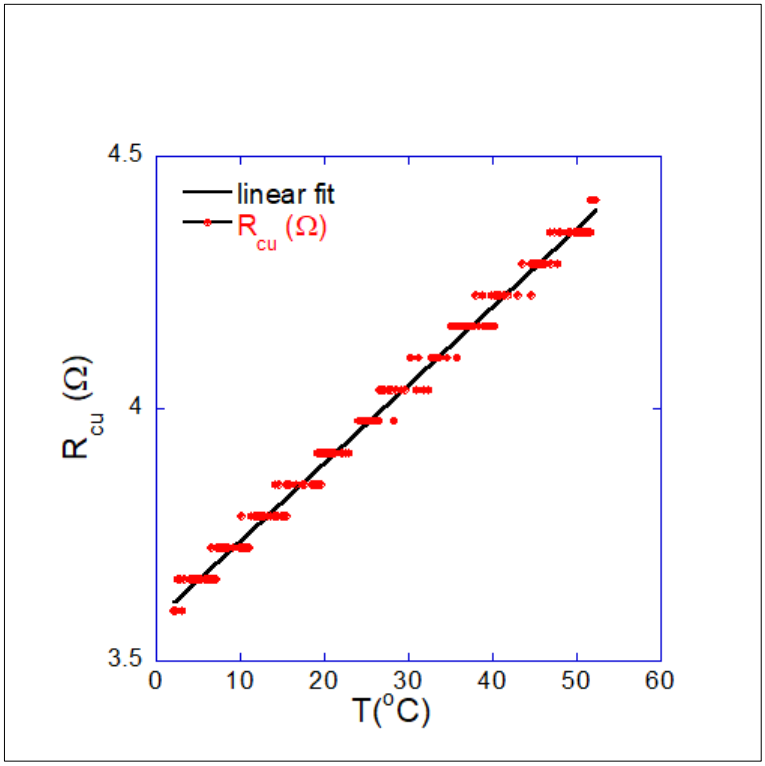

Fig 8: Temperature dependence of the resistance of a copper (Cu) wire. The red circles are the measured data points, and the line is the least-squares fit to the data. The step-like appearance of the data is due to the limited resolution of the measurement.

In metals the Fermi level falls within the conduction band, so there is an abundance of free electrons to conduct a current. The limiting factor for the conductivity is the presence of collisions between electrons and the rest of the crystal. While a part of the resistance is due to collisions with crystal imperfections that is temperature

independent, the linear dependence arises from the well-known lattice vibrations and is known as phonon scattering [39–41].

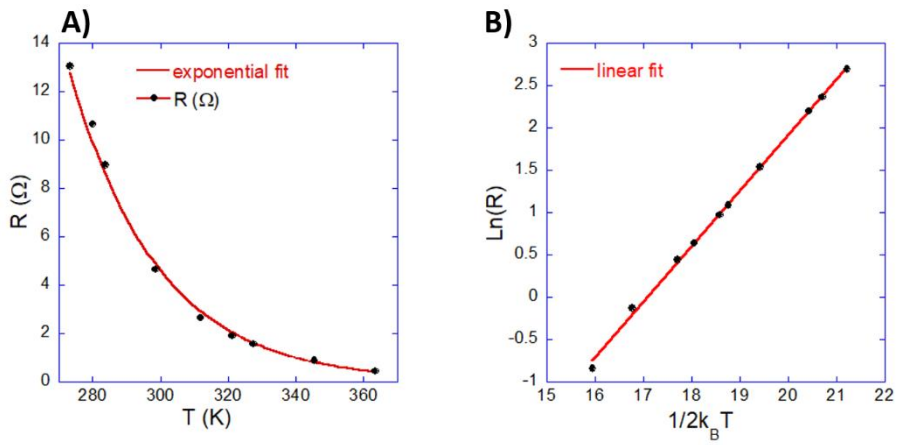

Fig. 9: Temperature dependence of resistance of a thermistor of type TTC-502. A) Raw data of the resistance of the thermistor as a function of the temperature along with a best fit exponential curve. B) Ln(R) as a function of ($1/2k_B$ T) where R is the resistance of the TTC-502 thermistor, e is the electron charge, k_B Boltzmann constant, and T is the absolute temperature.

Semiconductors, on the other hand have a much higher resistivity that varies exponentially with temperature, as seen in Fig. 9A. We used a type TTC-502 thermistor as a semiconductor and found its resistance to decrease rapidly with increasing the temperature. This behavior stems from the fact that the Fermi level falls between the valence band and the conduction band in semiconductors. For an intrinsic semiconductor at low-temperature, electrons will not have enough thermal energy to excite them into the conduction band and thus cannot contribute to the conductance since they are confined to the 'localized' valence band. As temperature increases, more electrons get thermally excited to the conduction band leaving behind a 'hole' for each of them. These electron-hole pairs contribute to conduction, and the resistance drops (i.e. the conductance increases) with the increase in their numbers. The probability of being thermally excited from a lower valence band to a higher energy level of the conduction band drops exponentially with the energy gap (E_g),

which is the energy difference between the two bands. So, the intrinsic carrier density (free charge- carrier density) is proportional to the Boltzmann factor $n_i(T) = Ae^{(\frac{-E_g}{2\,k_B T})}$, where k_B is the Boltzmann constant, A is a constant that depends on the semiconductor material, and T is the absolute temperature [30]. Assuming no significant change in the mobility, the conductance of the semiconductor is: $\sigma = en_i(T)\,(\mu_e + \mu_p)$, where $\mu_e\ and\ \mu_p$ are the electron and hole mobilities, respectively. The resistivity is $\rho(T) = \frac{1}{\sigma} = \frac{1}{Ae(\mu_e+\mu_p)}\ e^{(\frac{E_g}{2\,k_B T})}$, and thus the resistance has the form $R(T) = R_0 e^{(\frac{E_g}{2\,k_B T})}$, where R_0 is a constant.

Figure 9 B) shows a plot of the natural logarithm of the resistance, ln(R), as a function of $\frac{1}{2k_B T}$. Since $\ln(R) = \ln(R_0) + \frac{E_g}{2\,k_B T}$, the slope of this straight line is the energy gap (in eV) between the conduction and valence bands in the semiconductor. Our data shows an energy gap of (0.66 ± 0.01) eV, where the uncertainty is the 'standard deviation in the slope of the line, as obtained from the LINEST function in Excel'. This is within 1 % of the energy gap of germanium (0.67 eV) which is used in the TTC-502 thermistor [42].

We do caution that simply placing the thermistor in contact with the TEC surface will most likely give the wrong energy gap value, as it happened with our initial experiments. This is likely due to the poor thermal contact between the thermistor and the TEC plate. The thermistor has a painted surface and is shaped like a lentil seed and so does not lend itself to a good thermal contact with the flat TEC plate. Therefore the actual temperature of the thermistor seems to have been always closer to room temperature than the temperature registered by the thermocouple placed on the TEC surface. We solved this problem by placing the thermistor in a small water beaker placed on the TEC surface. Water insured a very good thermal contact with the thermistor and gave excellent results.

4.3 Further experiments

One main advantage of this experiment is that it lends itself naturally to being extended as an open-ended project, where students can easily augment the experiment

with different additions. Some possibilities that our students chose in the past were to connect a solar panel to power the TEC unit, to use a temperature control circuit like a Schmitt trigger to build a heating/cooling system, to use a hot coffee cup to produce electric energy, and multiple others.

5 CONCLUSION

Commercially available thermoelectric cooling devices have been used as simple and inexpensive tools to experiment with the Seebeck and Peltier thermoelectric effects. The temperature variation was found to follow Newton's law of cooling and heating. The cooling and heating ability of the devices was used to study the resistance change with temperature in a metal and a semiconductor by characterizing the temperature behavior for each of them, thus allowing us to extract the thermal coefficient of the resistance, α, for the metal and the energy gap, Eg, of the semiconductor. This experiment can be used as a sophomore electronics experiment or as an open-ended project in more advanced laboratories.

6 REFERENCES

[1] Halstead E 2016 Effects of reducing scaffolding in an undergraduate electronics lab *American Journal of Physics* **84**

[2] Zwickl B, Finkelstein N, Lewandowski H J, Rebello N S, Engelhardt P V and Singh C 2012 Transforming the advanced lab: Part I - Learning goals 2011 PHYSICS EDUCATION RESEARCH CONFERENCE (Omaha, NE) pp 391–4

[3] Nixon R S, Godfrey T J, Mayhew N T and Wiegert C C 2016 Undergraduate student construction and interpretation of graphs in physics lab activities *Phys. Rev. Phys. Educ. Res.* **12** 010104

[4] Zwickl B M, Finkelstein N and Lewandowski H J 2013 The process of transforming an advanced lab course: Goals, curriculum, and assessments *American Journal of Physics* **81** 63–70

[5] Tech Rep. 2014 AAPT Recommendations for the Undergraduate Physics Laboratory Curriculum

[6] Ashcroft N W, W A and Mermin N D 1976 *Solid State Physics* (Holt, Rinehart and Winston)

[7] Khandurina J, McKnight T E, Jacobson S C, Waters L C, Foote R S and Ramsey J M 2000 Integrated System for Rapid PCR-Based DNA Analysis in Microfluidic Devices *Anal. Chem.* **72** 2995–3000

[8] Yan J, Liao X, Yan D and Chen Y 2018 Review of Micro Thermoelectric Generator *Journal of Microelectromechanical Systems*

[9] Nolas G S, Sharp J and Goldsmid H J 2001 *Thermoelectrics: Basic Principles and New Materials Developments* vol 45 (Berlin, Heidelberg: Springer Berlin Heidelberg)

[10] Uchida K, Takahashi S, Harii K, Ieda J, Koshibae W, Ando K, Maekawa S and Saitoh E 2008 Observation of the spin Seebeck effect *Nature* **455** 778–81

[11] Xiao J, Bauer G E, Uchida K, Saitoh E and Maekawa S 2010 Theory of magnon-driven spin Seebeck effect *Physical Review B* **81** 214418

[12] Panitz J A 2002 Contemporary electronics: A focussed concept laboratory *American Journal of Physics* **70** 280–4

[13] Jewett J W and Serway R A 2014 *Physics for scientists and engineers with modern physics* (Brooks/Cole Cengage Learning)

[14] Seebeck T J 1922 *Abh. Dtsch. Akad. Wiss. Berl.* 265

[15] Peltier J C 1934 *Ann. Chim. Phys.* **56** 371

[16] Thomson W 1853 On the Dynamical Theory of Heat, with numerical results deduced from Mr Joule's Equivalent of a Thermal Unit, and M. Regnault's Observations on Steam *Earth and Environmental Science Transactions of The Royal Society of Edinburgh* **20** 261–88

[17] Thomson W 1857 On a mechanical theory of thermo-electric currents *Proceedings of the Royal society of Edinburgh* **3** 91–8

[18] Saitoh E, Ueda M, Miyajima H and Tatara G 2006 Conversion of spin current into charge current at room temperature: Inverse spin-Hall effect *Appl. Phys. Lett.* **88** 182509

[19] Rowe D M 2006 *Thermoelectrics handbook: macro to nano* (Boca Raton: CRC/Taylor & Francis)

[20] DiSalvo F J 1999 Thermoelectric Cooling and Power Generation *Science* **285** 703–6

[21] Akhanda M S, Rezaei S E, Esfarjani K, Krylyuk S, Davydov A V and Zebarjadi M 2021 Thermomagnetic properties of Bi_2Te_3 single crystal in the temperature range from 55 K to 380 K *Phys. Rev. Materials* **5** 015403

[22] Sinova J, Valenzuela S O, Wunderlich J, Back C H and Jungwirth T 2015 Spin Hall effects *Rev. Mod. Phys.* **87** 1213–60

[23] Tritt T M 2002 Thermoelectric Materials: Principles, Structure, Properties, and Applications *Encyclopedia of Materials: Science and Technology* (Elsevier) pp 1–11

[24] Ioffe A F, Stil'Bans L S, Iordanishvili E K, Stavitskaya T S, Gelbtuch A and Vineyard G 1959 Semiconductor thermoelements and thermoelectric cooling *PhT* **12** 42

[25] Turnbull D 1965 The Undercooling of Liquids *Scientific American* **212** 38–47

[26] Shaw R A, Durant A J and Mi Y 2005 Heterogeneous Surface Crystallization Observed in Undercooled Water *J. Phys. Chem. B* **109** 9865–8

[27] Yin L, Xia Q, Xue J, Yang S, Wang Q and Chen Q 2010 In situ investigation of ice formation on surfaces with representative wettability *Applied Surface Science* **256** 6764–9

[28] Vu T V, Tryggvason G, Homma S and Wells J C 2015 Numerical investigations of drop solidification on a cold plate in the presence of volume change *International Journal of Multiphase Flow* **76** 73–85

[29] Zhang H, Zhao Y, Lv R and Yang C 2016 Freezing of sessile water droplet for various contact angles *International Journal of Thermal Sciences* **101** 59–67

[30] Kittel C 2004 *Introduction to Solid State Physics* (New York: Wiley)

[31] Schuetze A P, Lewis W, Brown C and Geerts W J 2004 A laboratory on the four-point probe technique *American Journal of Physics* **72** 149–53

[32] Newton I 1701 Scala graduum caloris *Philos. Trans. Roy. Soc.(London)* **22** 824–9

[33] Besson U 2011 The cooling law and the search for a good temperature scale, from Newton to Dalton *Eur. J. Phys.* **32** 343–54

[34] Nesarajah M and Frey G 2016 Thermoelectric power generation: Peltier element versus thermoelectric generator *IECON 2016 - 42nd Annual Conference of the IEEE Industrial Electronics Society* IECON 2016 - 42nd Annual Conference of the IEEE Industrial Electronics Society (Florence, Italy: IEEE) pp 4252–7

[35] Hebei I T Datasheet - TEC1-12706

[36] Eid K F, Panth M and Sommers A D 2018 The physics of water droplets on surfaces: exploring the effects of roughness and surface chemistry *Eur. J. Phys.* **39** 025804

[37] Edalatpour M, Liu L, Jacobi A M, Eid K F and Sommers A D 2018 Managing water on heat transfer surfaces: A critical review of techniques to modify surface wettability for applications with condensation or evaporation *Applied Energy* **222** 967–92

[38] Boylestad R L 2010 *Introductory Circuit Analysis* (Prentice Hall)

[39] Bidwell C C 1940 Thermal Conductivity of Metals *Phys. Rev.* **58** 561–4

[40] Uher C 2004 Thermal Conductivity of Metals *Thermal Conductivity: Theory, Properties, and Applications* Physics of Solids and Liquids ed T M Tritt (Boston, MA: Springer US) pp 21–91

[41] Sham L J and Ziman J M 1963 The electron-phonon interaction *Solid State Physics* vol 15 (Elsevier) pp 221–98

[42] NTC Thermistor TTC05 Series datasheet catalog

Appendices

Appendix A: Python Code used to find the amplitudes of the oscillations

```
import matplotlib.pyplot as plt

import pandas as pd

W = pd.read_excel (r'F:\Rand\BZU\Research\Physical Pendulum Viscometer\Data\Water
V2 40g.xlsx')

W1 = W.iloc[:,0]

W2 = 10000*W.iloc[:,1]

peaks = []

n=50

maxes = []

time = []

for i in range (n,len(W2)-n):

   x2 = max(W2[i-n:i+n])

   if x2 == W2 [i]:

      t2 = W1 [i]

      peaks.append(i)

      maxes.append(x2)

      time.append(t2)

data = {'amp': maxes, 'time': time}

df2 = pd.DataFrame(data, columns = ['amp', 'time'])

df2.to_excel(r'F:\Rand\BZU\Research\Physical Pendulum Viscometer\Data\water amp
1.xlsx')

plt.plot(W1[peaks], W2[peaks], 'bs',linewidth=2.0, label=' In Water')

plt.grid(True, linestyle='-.')

plt.tick_params(labelsize='large', width=3)
```

```
plt.ylabel('Amp. (deg.) ',size = 20 )

plt.xlabel('Time (Sec.) ',size = 20)

plt.legend(loc='upper right')

plt.show()
```

Appendix B: The Block Diagram of The LabView Program

In this appendix, we present a magnification of Figure 3.6 to illustrate it.

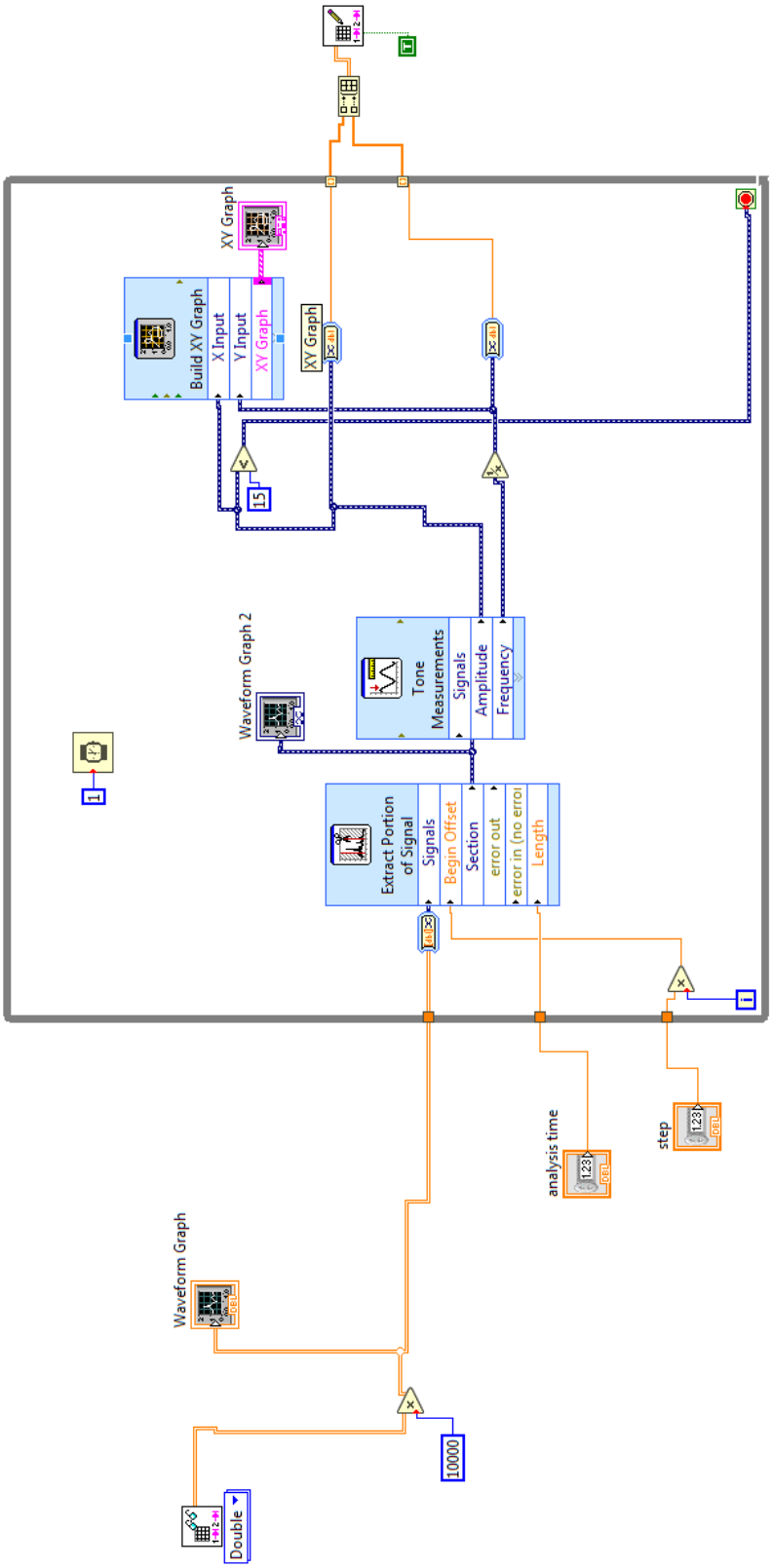

Figure B.0.1: A snapshot of the "LabView Program" block diagram screen (Zoomed)